

# Acoustic radiation potential on a sphere in plane, cylindrical, and spherical standing wave fields<sup>a)</sup>

M. Barmatz

*Jet Propulsion Laboratory, California Institute of Technology, Pasadena, California 91109*

P. Collas

*Department of Physics and Astronomy, California State University, Northridge, Northridge, California 91330*

(Received 2 April 1984; accepted for publication 12 September 1984)

We have applied the method of Gor'kov for deriving the acoustic radiation potential on a sphere in an arbitrary sound field. Generalized potential and force expressions are derived for arbitrary standing wave modes in rectangular, cylindrical, and spherical geometries for the case where the sphere radius is much smaller than the wavelength ( $kR \ll 1$ ). Criteria for determining radiation potential minima are derived and examples of characteristic spatial radiation potential profiles are presented. Single modes that can sustain stable positioning are discussed for each geometry. The localizing force strengths for representative standing wave modes in the three geometries are also compared. In this paper, we consider the positioning of samples due to acoustic forces only. However, the method developed here is general and can be extended to include gravity or other external forces.

PACS numbers: 43.25.Qp, 43.25.Gf, 43.40.Qi, 43.20.Ks

## INTRODUCTION

An object in the presence of a sound field will experience forces associated with the field. Kundt<sup>1</sup> was one of the first to observe the effect of acoustic forces through measurements on the motion of dust particles in resonant tubes. A detailed theoretical understanding of acoustic forces was first presented by King<sup>2</sup> for a rigid sphere in a plane standing or progressive wave field in an ideal fluid. King calculated the radiation force by summing the effect of acoustic pressures acting on each surface element of the rigid sphere. Yosioka and Kawasima<sup>3</sup> extended this method to include the effects of a compressible sphere. King's theory was verified experimentally for liquid<sup>4</sup> and gaseous<sup>5,6</sup> media.

King's approach was later extended by Embleton to the case of a rigid sphere in a progressive spherical<sup>7</sup> or cylindrical<sup>8</sup> wave field. In an ingenious paper Gor'kov,<sup>9</sup> using a different approach than King, derived a simple method to determine the forces acting on a particle in an *arbitrary* acoustic field. Gor'kov showed that his expression was equivalent to King's in the case of a plane standing wave. Nyborg<sup>10</sup> also derived simple expressions for the acoustic force by extending the methods of King<sup>2</sup> and Embleton.<sup>7</sup> In the case of standing waves, Nyborg's expression reduced to that of Gor'kov.<sup>9</sup> Several additional references are given in an excellent review of high intensity sound fields by Rosenberg.<sup>11</sup>

The ability to influence the motion of objects by a sound field has many applications.<sup>12</sup> At this time, NASA is supporting the development of acoustic positioning techniques<sup>13</sup> for the processing of materials in the low gravity environment of space. We define positioning as the ability to localize a sample at a position interior to the chamber bound-

aries. The motivation for this investigation comes from the need to understand in detail the acoustic localization capabilities of various resonator geometries. The main emphasis is to determine those normal modes that will sustain stable acoustic positioning of small samples.

In this paper, we will develop general acoustic radiation potential and force expressions for standing waves in rectangular, cylindrical, and spherical geometries. In Sec. I, we present Gor'kov's general expression which is used to evaluate the acoustic radiation force in an arbitrary sound field. The range of validity of Gor'kov's results is discussed, and a method for determining the critical points of the potential is introduced. General radiation potential expressions are then derived in Sec. II for resonance modes in a rectangular geometry. Selection rules for potential minima (localization positions) are developed, and examples of characteristic spatial profiles are presented. In Secs. III and IV, we extend the calculations to standing waves in cylindrical and spherical geometries, respectively. New positioning modes for these geometries will be discussed. A comparison of the positioning capabilities of standing waves in the three geometries is given in Sec. V. Finally, Sec. VI contains a brief summary and conclusions. Preliminary results of this investigation were reported previously.<sup>14</sup>

## I. THEORY

Gor'kov<sup>9</sup> derived a very useful expression for the potential  $U$  of the acoustic force  $F$  that acts on a small spherical particle in an arbitrary acoustic field in an ideal fluid. Gor'kov worked within the framework of the linear theory; thus the time-averaged force on the particle is correct up to terms of second order in the fluid particle velocity. The velocity potential  $\Phi$  was represented as the sum of an incident and a scattered term

$$\Phi = \Phi_{in} + \Phi_{sc}.$$

<sup>a)</sup>The research described in this paper was carried out by the Jet Propulsion Laboratory, California Institute of Technology, under contract with the National Aeronautics and Space Administration.

Gor'kov assumed that the radius of the spherical particle  $R \ll \lambda$ , where  $\lambda$  is the wavelength of the sound.<sup>15</sup> Then using results derived in Landau and Lifshitz,<sup>16</sup>  $\Phi_{sc}$  was expressed entirely in terms of incident field quantities. In addition, the compressibility of the particle and the possibility that it may be set in motion by the incident wave was taken into account.<sup>17</sup> After considerable algebra,<sup>18</sup> Gor'kov finally obtained the expression for the time-averaged potential  $U$ .

$$U = 2\pi R^3 \left[ \left( \overline{p_{in}^2} / 3\rho c^2 \right) f_1 - \left( \rho \overline{v_{in}^2} / 2 \right) f_2 \right], \quad (1)$$

where  $\overline{p_{in}^2}$  and  $\overline{v_{in}^2}$  are the mean-square fluctuations of the pressure and velocity in the wave at the point where the particle is located. In terms of the velocity potential we have

$$p_{in} = - \frac{\rho \partial \Phi_{in}}{\partial t}, \quad (2)$$

$$v_{in} = \text{grad } \Phi_{in}. \quad (3)$$

The factors  $f_1$  and  $f_2$  appearing in Eq. (1) are given by

$$f_1 = 1 - \rho c^2 / \rho_s c_s^2, \quad f_2 = 2(\rho_s - \rho) / (2\rho_s + \rho), \quad (4)$$

where  $c$  is the speed of sound in the fluid,  $c_s$  is the speed of sound in the particle,  $\rho$  is the density of the fluid, and  $\rho_s$  is the density of the particle. The allowable range of the factors  $f_1$  and  $f_2$  are  $-\infty < f_1 < 1$  and  $-2 < f_2 < 1$ . In the case of a rigid sphere  $f_1 = f_2 = 1$ . The acoustic force components are obtained from the potential using the expression

$$\mathbf{F} = - \text{grad } U. \quad (5)$$

For comparison and computational purposes, we define the following dimensionless expressions for the radiation potential, force components, acoustic pressure, and particle velocity:

$$\begin{aligned} \tilde{U} &= U / (\pi R^3 \rho v_0^2), \quad \tilde{F}_i = F_i / (\pi R^3 \rho v_0^2 k), \\ \tilde{p} &= p_{in} / \rho c v_0, \quad \tilde{v} = v_{in} / v_0, \end{aligned} \quad (6)$$

where  $v_0$  is the maximum particle velocity.

We emphasize that Eq. (1) is valid for  $R \ll \lambda$ ; in fact it is correct to lowest order in  $R/\lambda$ , i.e.,  $(R/\lambda)^3$ . Furthermore, as mentioned above, Eq. (1) is applicable to any acoustic field with the exception of fields similar to a plane traveling wave. In the latter case, the contribution to the force is much smaller,<sup>9</sup> of the order of  $(R/\lambda)^6$ . Gor'kov did not consider multiple scattering effects; thus this analysis becomes increasingly less precise as the chamber walls are approached. Gor'kov showed that in the case of a rigid sphere in a plane standing wave field, Eq. (1) gave an expression for the force that is identical to the corresponding one derived by King.<sup>2</sup> As an additional application of Eq. (1), Gor'kov gave the expression for the potential  $U$  in the case of a spherical (converging or diverging) wave. Embleton<sup>7</sup> has also calculated the radiation force on a sphere due to a diverging spherical wave without restriction to  $R/\lambda \ll 1$ . Embleton goes on to evaluate his expression for the radiation force in detail for the rigid sphere case  $f_1 = f_2 = 1$ , as a double expansion in powers of  $(1/kr \sim \lambda/r)$  and  $(kR \sim R/\lambda)$ . There are only a finite number of terms to any given order in  $R/\lambda$ ; thus, one would expect Gor'kov's expression to agree with Embleton's lowest order terms, i.e., to order  $(R/\lambda)^3$ . This is indeed the case, apart from a couple of misprints and taking into ac-

count Embleton's different sign convention.<sup>19</sup>

For a given mode, the stable localization positions correspond to particular minima of the potential  $\tilde{U}$ . The critical points of the potential are obtained by requiring

$$\frac{\partial \tilde{U}}{\partial \tilde{x}_i} = 0, \quad (7)$$

or equivalently  $\tilde{F}_i = 0$ , where  $\tilde{x}_i = kx_i$  for dimensioned  $x_i$  coordinates. To test the nature of these critical points, we must evaluate the eigenvalues of the Hessian matrix  $H\tilde{U}$  consisting of all possible second partial derivatives of the potential at the positions given by Eq. (7). A critical point is a nondegenerate maximum if all the eigenvalues are negative and it is a nondegenerate minimum if all the eigenvalues are positive. Combinations of positive and negative eigenvalues lead to various types of saddle points while one or more zero eigenvalues yield degenerate critical points (see Appendix A).

For practical applications of acoustic positioning, it is important to know the degree of stability provided by a radiation potential well. When random external forces are present, a sample will move away from the potential minimum. If the external force is small, the degree of sample stability will depend on the strength of the acoustic restoring force near the potential minimum. In general, the potential well is not symmetric, and there will be characteristic directions that correspond to the weakest restoring forces. The maximum restoring force  $\tilde{F}_{max}$  along any particular direction occurs at the inflection points between the potential maxima and minima.

In the neighborhood of a nondegenerate minimum, the potential energy and forces may be written in a form identical to that of a three-dimensional anisotropic harmonic oscillator (see Appendix B).

$$\tilde{U} = \frac{1}{2} \sum_{i=1}^3 \tilde{\kappa}_i \tilde{x}_i^2, \quad \tilde{F}_i = -\tilde{\kappa}_i \tilde{x}_i, \quad (8)$$

where the restoring force constants  $\tilde{\kappa}_i$  are

$$\tilde{\kappa}_i = \frac{\partial^2 \tilde{U}}{\partial \tilde{x}_i^2}. \quad (9)$$

These dimensionless restoring force constants are useful quantities for comparing the positioning capabilities of various potential minima for modes of the same or different geometries.

In Secs. II-IV, we will develop the radiation potential and force expressions specific to chambers of rectangular, cylindrical, and spherical geometry. The three coordinate variables of a given geometry will each define nodal force surfaces. Potential minima correspond to the intersection of certain nodal force surfaces determined by selection rules. In most cases, these minima will be isolated points, lines, or surfaces depending on whether the normal mode is a function of three, two, or one of the coordinate variables, respectively. However, for cylindrical and spherical geometries, there are special modes of only two coordinate variables that have isolated minima points. These special modes are important for acoustic positioning applications and will be discussed in detail. The notation used for the rectangular, cylin-

TABLE I. Notation for parameters in rectangular, cylindrical, and spherical coordinate systems.

	Rectangular	Cylindrical	Spherical
coordinates	$x, y, z$	$\phi, r, z$	$\theta, r, \phi$
quantum numbers <sup>a</sup>	$n_x, n_y, n_z$	$m, n, n_z$	$l, n, m$
dimensions	$l_x, l_y, l_z$	$a, l_z$	$r_0$
wavenumbers	$k_i = \pi n_i / l_i$	$k_r = \pi \alpha_{mn} / a$ $k_z = \pi n_z / l_z$	$k = \pi \gamma_{lm} / r_0$

<sup>a</sup> All quantum numbers are non-negative integers beginning with zero.

dical, and spherical geometries discussed in this paper are given in Table I.

## II. RECTANGULAR GEOMETRY

We will first investigate the critical points of the radiation potential for a rectangular chamber. We shall be mainly interested in the location of the minima and the behavior of the potential near the minima. For rectangular geometries, a spatial position is designated by the  $x, y$ , and  $z$  coordinates,  $(xyz)$ , and a normal mode is given by the integer quantum numbers  $n_x, n_y, n_z, (n_x, n_y, n_z)$ .<sup>20</sup> The origin (000) for the rectangular coordinate system is chosen to be at a corner of the chamber.

The velocity potential for a standing wave field in a rectangular chamber of dimensions  $l_x, l_y, l_z$  is

$$\Phi_{in} = - (v_0/k) \cos k_x x \cos k_y y \cos k_z z \sin \omega t, \quad (10)$$

where the wavenumber  $k$  is

$$k = (\omega/c) = (k_x^2 + k_y^2 + k_z^2)^{1/2}, \quad (11)$$

and

$$k_x = \frac{\pi n_x}{l_x}, \quad k_y = \frac{\pi n_y}{l_y}, \quad \text{and} \quad k_z = \frac{\pi n_z}{l_z}. \quad (12)$$

The dimensionless acoustic pressure and particle velocity for a rectangular normal mode are

$$\tilde{p} = \cos k_x x \cos k_y y \cos k_z z \cos \omega t, \quad (13)$$

and

$$\tilde{v} = [(k_x/k)^2 \sin^2 k_x x \cos^2 k_y y \cos^2 k_z z + (k_y/k)^2 \cos^2 k_x x \sin^2 k_y y \cos^2 k_z z + (k_z/k)^2 \cos^2 k_x x \cos^2 k_y y \sin^2 k_z z]^{1/2} \sin \omega t. \quad (14)$$

Substituting the mean-square values of the pressure and velocity into Gor'kov's expression [Eq. (1)] yields the dimensionless potential:

$$\begin{aligned} \tilde{U} = & (f_1/3) \cos^2 k_x x \cos^2 k_y y \cos^2 k_z z \\ & - (f_2/2) [(k_x/k)^2 \sin^2 k_x x \cos^2 k_y y \cos^2 k_z z \\ & + (k_y/k)^2 \cos^2 k_x x \sin^2 k_y y \cos^2 k_z z \\ & + (k_z/k)^2 \cos^2 k_x x \cos^2 k_y y \sin^2 k_z z]. \end{aligned} \quad (15)$$

The dimensionless force component  $\tilde{F}_x$ , obtained from the spatial derivatives of the potential, is given by

$$\begin{aligned} \tilde{F}_x = & \left( \frac{k_x}{k} \right) \sin 2k_x x \left\{ \left[ \frac{f_1}{3} + \left( \frac{f_2}{2} \right) \left( \frac{k_x}{k} \right)^2 \right] \right. \\ & \times \cos^2 k_y y \cos^2 k_z z - \left. \left( \frac{f_2}{2} \right) \left[ \left( \frac{k_y}{k} \right)^2 \sin^2 k_y y \right. \right. \\ & \left. \left. \times \cos^2 k_z z + \left( \frac{k_z}{k} \right)^2 \cos^2 k_y y \sin^2 k_z z \right] \right\}. \end{aligned} \quad (16)$$

To obtain  $\tilde{F}_y$  and  $\tilde{F}_z$ , simply interchange  $x \leftrightarrow y$  and  $x \leftrightarrow z$ , respectively, in Eq. (16).

The normal modes  $(n_x, n_y, n_z)$  of a rectangular chamber may be divided into three categories<sup>20</sup> corresponding to (i) oblique modes having no  $n$  values zero, (ii) tangential modes having one  $n$  value zero, and (iii) axial modes having two  $n$  values zero. The critical points of these modes naturally separate into two sets. For the  $x$  coordinate, one set corresponds to  $\sin 2k_x x = 0$ , i.e.,

$$\sin k_x x = 0, \quad \cos k_x x = 0, \quad (17)$$

with similar expressions for the  $y$  and  $z$  coordinates. The positions of these critical points are given by

$$\frac{x}{l_x} = \frac{m_x}{2n_x}, \quad \frac{y}{l_y} = \frac{m_y}{2n_y}, \quad \frac{z}{l_z} = \frac{m_z}{2n_z}, \quad (n_x, n_y, n_z \neq 0), \quad (18)$$

where  $m_x, m_y$ , and  $m_z$  are non-negative integers less than or equal to  $2n_x, 2n_y$ , and  $2n_z$ , respectively. This condition is valid for oblique, tangential, and axial modes. The nature of the critical points is determined from the evenness and oddness of  $m_x, m_y$ , and  $m_z$  as discussed in Appendix A. Unless otherwise stated, in the remainder of this paper we will limit ourselves to cases where the compressibility of the sample is less than and the density of the sample is greater than those of the surrounding medium, i.e.,  $f_1 > 0$  and  $f_2 > 0$ . Under these constraints, the positions of nondegenerate (isolated) potential minima are the intersection of the  $x, y$ , and  $z$  nodal force planes corresponding to having one  $m$  odd and the others even. When all the  $m$  values are even, the critical points are maxima, and when all the  $m$  values are odd, the critical points are degenerate. These coordinate selection rules for axial, tangential, and oblique rectangular modes are given in Table II. The positions of these critical points are independent of the sample characteristics (i.e.,  $f_1$  and  $f_2$ ); however, their type and the magnitude of the potential do

TABLE II. Potential minima nodal force surfaces for various modes in rectangular geometry.

Mode	$x$	$y$	$z$
axial (00 $n_z$ )	...	...	$\cos k_z z = 0$
tangential ( $n_x$ 0 $n_z$ )	$\sin k_x x = 0$ $\cos k_x x = 0$	...	$\cos k_z z = 0$ $\sin k_z z = 0$
oblique ( $n_x n_y n_z$ )	$\cos k_x x = 0$ $\sin k_x x = 0$	$\sin k_y y = 0$ $\cos k_y y = 0$	$\sin k_z z = 0$ $\cos k_z z = 0$

depend on  $f_1$  and  $f_2$ . The magnitude of the potential at these maxima and minima are

$$\tilde{U}_{\max} = \frac{f_1}{3}, \quad \tilde{U}_{\min} = -\left(\frac{f_2}{2}\right)\left(\frac{k_i}{k}\right)^2, \quad (19)$$

where the subscript  $i$  corresponds to the odd  $m$  direction. The magnitudes  $\tilde{U}_{\max}$  and  $\tilde{U}_{\min}$  are reduced for nonrigid spherical samples ( $f_1 < 1, f_2 < 1$ ).

The second set of critical points comes from the zeros of the term in braces in Eq. (16). These points, which only arise for tangential and oblique modes, are either nondegenerate saddle points or degenerate critical points. Thus the only nondegenerate (isolated) potential minima arise for oblique normal modes of a rectangular chamber with coordinates satisfying Eq. (18) with one  $m$  odd and the other two even.

To illustrate the acoustic behavior of these rectangular chamber modes, we consider some representative cases. For the simple case of the  $(00n_z)$   $z$ -axial or plane-wave mode,  $\tilde{p}$ ,  $\tilde{U}$ , and  $\tilde{F}_z$  are given by

$$\tilde{p}(z) = \cos k_z z \cos \omega t, \quad (20)$$

$$\tilde{U}(z) = (f_1/3)\cos^2 k_z z - (f_2/2)\sin^2 k_z z, \quad (21)$$

$$\tilde{F}_z(z) = [(f_1/3) + (f_2/2)]\sin 2k_z z. \quad (22)$$

The force expression, Eq. (22), is equivalent to that derived by King<sup>2</sup> and Yosioka and Kawasima<sup>3</sup> for a plane standing wave. The results discussed here for the  $(00n_z)$   $z$ -axial mode are also applicable to the  $(n_x 00)$  and  $(0n_y 0)$  modes.

The spatial dependence of these functions for the  $(001)$   $z$ -axial mode is shown in Fig. 1 for the case of a stationary rigid sphere. The extrema of the potential, where the force is zero, occur at the reflecting walls ( $z/l_z = 0$  or  $1$ ) and the midplane ( $z/l_z = 0.5$ ). The forces associated with this plane-wave sound field will position a small sample at the midplane, where the potential is a minimum. The excitation of the  $n_z$  th harmonic  $z$ -axial mode will produce zero force components at the reflecting walls and  $n_z$  potential minima planes in the interior of the resonator with coordinates given by Eq. (18) for  $m_z$  odd.

The shape of the radiation potential well is strongly dependent on the magnitude and sign of the variables  $f_1$  and  $f_2$ . The positions of the potential minima for a plane-wave mode are located at pressure nodes or antinodes depending only on the signs of  $f_1$  and  $f_2$  as shown in Table III. When the sample density is greater than the surrounding medium ( $f_2 > 0$ ), the potential minima coincide with pressure nodes, while for sample densities less than the surrounding fluid ( $f_2 < 0$ ), these minima occur at pressure antinodes. To illustrate these results, we show in Fig. 2 the radiation potential and force of the fundamental  $z$ -axial plane-wave mode for an air bubble in water. This curve corresponds to a bubble smaller than resonant size.

It is clear from the above discussion that an axial or plane-wave mode cannot localize a sample at unique positions in the resonator interior. However, the modes can position a sample within a plane normal to the mode wave vector. The localization of a sample at a unique position can be attained by the simultaneous excitation of three orthogonal axial modes, in which case the intersection of the three sets of orthogonal planes is a set of points within the resonator inte-

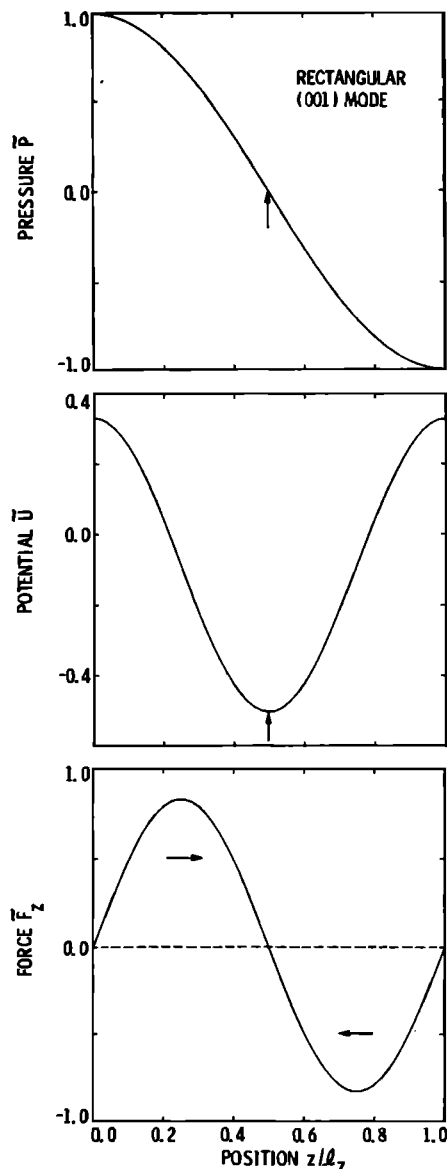


FIG. 1. Position dependence of the acoustic pressure, potential, and force on a rigid sphere for the  $(001)$   $z$ -axis rectangular mode. The potential minimum plane is midway between the reflecting  $z$  walls and corresponds to the pressure nodal plane.

rior. This positioning technique was demonstrated experimentally<sup>21</sup> for a rectangular chamber and is now being developed further for NASA's Microgravity Science and Applications program.<sup>13</sup>

Let us now consider an  $(n_x 0n_z)$   $x, z$ -tangential mode. The results discussed here are also applicable to the  $(n_x n_y 0)$  and  $(0n_y n_z)$  modes. The acoustic potential for this mode exhibits different behavior than was obtained for the axial

TABLE III. Dependence of the potential minima location on the sign of  $f_1$  and  $f_2$  for a plane-wave rectangular mode.

$f_1$	$f_2$	Location of minima
positive	zero, positive	pressure node
zero, negative	positive	pressure node
zero, positive	negative	pressure antinode
negative	zero, negative	pressure antinode

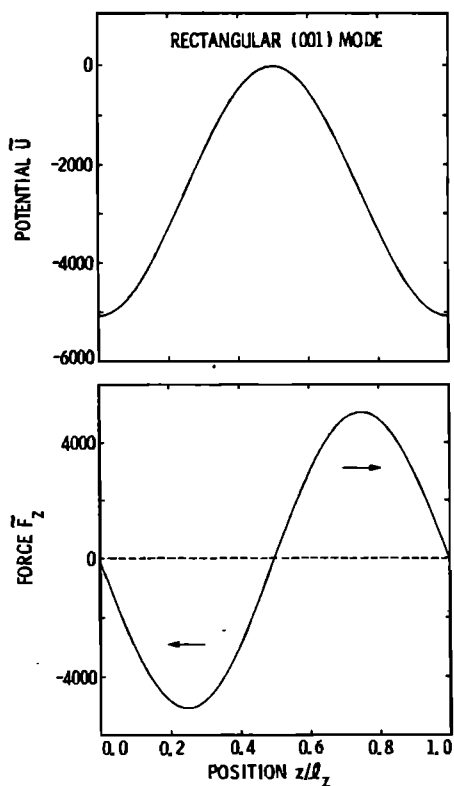


FIG. 2. Position dependence of the acoustic potential and force on an air bubble (smaller than resonant size) in water for the (001) z-axial rectangular mode. The potential minima planes now correspond to the reflecting z walls which are pressure antinodal planes.

modes due to the effects of the coupling between the x and z propagation directions. The values of  $\bar{U}$  at the minima are always less than the critical value  $-0.5$  obtained for the axial modes. Decreasing the chamber aspect ratio  $l_z/l_x$  will further reduce the depth of the potential minima. For these modes the potential minima positions are all nonisolated lines, most of which lie on the walls of the chamber. The lowest-order tangential mode that has an interior minimum line is the (102), where the potential minimum is along the chamber axis ( $x/l_x = 0.5$  and  $z/l_z = 0.5$ ). Figure 3 shows an  $x,z$ -contour graph of the potential on a rigid sphere for the (102) mode. This mode has seven minima lines along the  $y$  direction, with six of these being on the walls. The interior potential well is asymmetric, being steeper in the  $z$  direction. As was the case for an axial mode, the (102) tangential mode cannot localize a sample at a unique position, since one of its mode eigenvalues ( $n_y$ ) is zero. Localization at a unique position can again be attained by the simultaneous excitation of two modes, which together provide appropriate forces in the three orthogonal directions. For example, exciting the (102) tangential mode and the (010) axial mode will produce a unique localization position at the center of the chamber.

The oblique modes ( $n_x, n_y, n_z$ ) exhibit the most complicated radiation potential structure. These modes have *isolated* potential minima points with almost all of these positioned at the chamber walls. The lowest-order oblique mode that has an interior potential minimum is the (221), or equivalently the (122) or (212). Figure 4 shows hidden line graphs for the (221) mode potential in the center planes  $y/l_y = 0.5$  and  $z/l_z = 0.5$ . There are 33 potential minima for this mode,

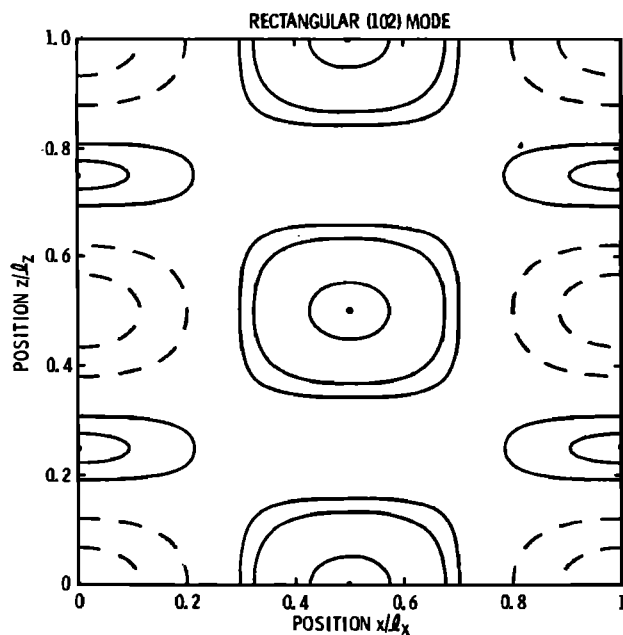


FIG. 3.  $x,z$ -contour graph of the acoustic potential for the (102)  $x,z$ -tangential rectangular mode. There are seven nonisolated potential minima lines; six are along the walls, and the deepest minima ( $x/l_x = z/l_z = 0.5$ ) goes through the chamber center. The solid lines depict contours near the minima, while the dashed lines correspond to contours near the maxima.

with 32 on the walls and one at the chamber center ( $x/l_x = 0.5$ ,  $y/l_y = 0.5$ , and  $z/l_z = 0.5$ ). The depth of the interior potential well depends on the aspect ratios  $l_y/l_x$  and  $l_z/l_x$ . It is clearly seen from these plots that the chamber center position is an isolated potential minimum. There are also higher-order oblique modes that have isolated minima in the interior of the chamber. For example, the ( $n_x 21$ ) modes with  $n_x > 2$

#### RECTANGULAR (221) MODE

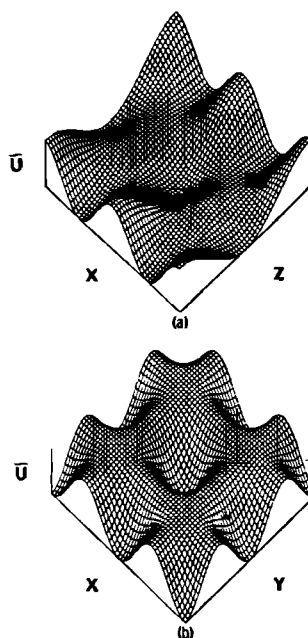


FIG. 4. Hidden line graphs of acoustic potential for the (221) rectangular mode. (a)  $y/l_y = 0.5$  center plane. There are six isolated minima on the  $x$  and  $z$  walls and one in the center. (b)  $z/l_z = 0.5$  center plane. There are eight isolated minima on the  $x$  and  $y$  walls and one in the center.

TABLE IV. Characteristics of potential minima for a rigid sphere for various modes in rectangular geometry.

Mode	Surface	$\bar{U}$ critical value	Location	Number of minima
axial (00 $n_z$ )	plane	- 1/2	interior and walls	$n_z$
tangential* ( $n_x$ 0 $n_z$ )	line	$-(k_i/k)^2/2$	interior and walls	$2n_x n_z - n_x - n_z$
			walls	$2(n_x + n_z)$
oblique ( $n_x n_y n_z$ )	point	$-(k_i/k)^2/2$	interior	$3n_x n_y n_z - 2(n_x n_y + n_y n_z + n_x n_z)$
			walls	$4(n_x n_y + n_y n_z + n_x n_z)$

\*  $k_i$  corresponds to  $k_x$  or  $k_y$  (tangential mode) or  $k_x, k_y,$  or  $k_z$  (oblique mode). The subscript  $i$  denotes which variable has  $k_i x_i = 0$ .

have  $n_x - 1$  interior minima at positions  $x/l_x = m_x/2n_x, y/l_y = 0.5,$  and  $z/l_z = 0.5,$  with  $m_x = 2, 4, \dots, 2n_x - 2$ . A summary of radiation potential minima characteristics for axial, tangential, and oblique rectangular modes is given in Table IV.

### III. CYLINDRICAL GEOMETRY

In a cylindrical chamber of radius  $a$  and length  $l_z,$  a spatial position is designated by the  $\phi, r,$  and  $z$  coordinates ( $\phi r z$ ) and a normal mode is given by the quantum numbers  $m, n,$  and  $n_z, (m n n_z).$ <sup>20</sup> Other important notations for cylindrical geometries are given in Table I. The origin (000) for the cylindrical coordinate system is chosen to be at the center of a  $z$  wall. The conversion from the lower symmetry of rectangular geometry to the higher symmetry of cylindrical geometries leads to new positioning features. The  $x, y$  Cartesian coordinates and  $n_x$  and  $n_y$  quantum numbers are transformed into the  $\phi, r$  polar coordinates and  $m$  and  $n$  quantum numbers, respectively. In rectangular resonators, the acoustic properties of a given mode are independent of  $x$  or  $y$  as long as either  $n_x$  or  $n_y$  are zero. This is not the case in the cylindrical system, where all non- $z$ -axial modes are  $r$  dependent regardless of the  $m$  and  $n$  values. Furthermore, since there are no reflecting boundaries for cylindrical  $\phi$  waves, the velocity potential for a standing wave field in a cylindrical chamber contains an arbitrary phase constant  $\phi_0$  (Ref. 22) and is given by

$$\Phi_{in} = -(v_0/k) J_m(k_r r) \cos(m\phi + \phi_0) \cos k_z z \sin \omega t, \quad (23)$$

where the wavenumber  $k$  is specified by

$$k = \omega/c = (k_r^2 + k_z^2)^{1/2}, \quad (24)$$

with

$$k_r = \pi \alpha_{mn}/a, \quad k_z = \pi n_z/l_z. \quad (25)$$

Assuming rigid boundary conditions,  $\alpha_{mn}$  is a solution of the relation  $d [j_m(\pi \alpha)]/d\alpha = 0,$  where  $J_m$  is the Bessel function of order  $m$ . Since  $\phi_0$  is an arbitrary phase constant, we will let  $\phi_0 = 0$  in the following calculations of acoustic properties. After calculating the mean-square fluctuations of the acoustic pressure and particle velocity and substituting into Eq. (1), we obtain the following expression for the dimensionless radiation potential of the ( $m n n_z$ ) normal mode,

$$\begin{aligned} \bar{U} = & \left(\frac{f_1}{3}\right) J_m^2(\chi) \cos^2 m\phi \cos^2 k_z z - \left(\frac{f_2}{2}\right) \left[\left(\frac{k_r}{k}\right)^2 \left[\left(\frac{m J_m(\chi)}{\chi}\right)^2\right.\right. \\ & \left.\left. - J_{m+1}(\chi) \left(\frac{2m J_m(\chi)}{\chi} - J_{m+1}(\chi)\right) \cos^2 m\phi\right] \cos^2 k_z z\right. \\ & \left. + J_{m+1}^2\left(\frac{k_z}{k}\right) \cos^2 m\phi \sin^2 k_z z\right], \quad (26) \end{aligned}$$

where  $\chi = k_r r.$

The dimensionless force components for a cylindrical chamber are obtained using the following expressions:

$$\bar{F}_r = -\frac{\partial \bar{U}}{\partial r}, \quad (27)$$

$$\bar{F}_\phi = -\bar{r}^{-1} \left(\frac{\partial \bar{U}}{\partial \phi}\right), \quad (28)$$

$$\bar{F}_z = -\frac{\partial \bar{U}}{\partial z}, \quad (29)$$

where  $\bar{r} = kr$  and  $\bar{z} = kz.$  Explicit expressions for these force components are given in Appendix C.

The normal modes of a cylindrical chamber may also be categorized in terms of axial, tangential, and oblique modes as was done for the rectangular modes. The  $z$ -axial modes, corresponding to  $m = n = 0,$  have motion only along the  $z$  axis while the  $r$ -axial modes, for which  $m = n_z = 0,$  have entirely radial motion and focus the sound along the cylinder axis. The  $\phi$ -axial modes, with  $n = n_z = 0,$  travel close to the curved walls, having little motion near the cylindrical axis. Modes for which only  $n_z = 0$  move parallel to the walls of the chamber and may be called  $\phi, r$ -tangential modes.

The potential minima (localization positions) for cylindrical modes are determined by the intersection of particular sets of nodal force surfaces. The types of nodal force surfaces for cylindrical geometries are shown at the bottom of Table V. The  $z$ -nodal force surfaces are circular planes defined by

$$\cos k_z z = 0 \text{ or } \sin k_z z = 0, \quad (30)$$

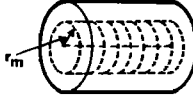
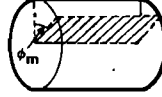
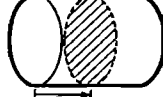
with  $z$  coordinates given by Eq. (18). The  $\phi$ -nodal force surfaces are rectangular half-planes defined by

$$\cos m\phi = 0 \text{ or } \sin m\phi = 0. \quad (31)$$

In analogy with the rectangular coordinate definitions, these positions are given by

$$\phi/2\pi = q/4m, \quad (32)$$

TABLE V. Potential minima nodal force surfaces for various modes in cylindrical geometry.

Mode	$r$	$\phi$	$z$
$z$ axial ( $00n_z$ )	...	$\sin m\phi = 0$	$\cos k_z z = 0$
$r$ axial ( $0m0$ ) and tangential* ( $0mn_z$ )	$J_2(\chi) - [(4f_1/3f_2) + 1]J_0(\chi) = 0$ $J_1(\chi) = 0$	$\sin m\phi = 0$ $\sin m\phi = 0$	$\sin k_z z = 0$ $\cos k_z z = 0$
oblique* ( $mn_n$ )	$(m+1)J_{m+1}(\chi) - (m-1)J_{m-1}(\chi) = 0$ $J_m''(\chi) - (2f_1/3f_2)(k/k_r)^2 J_m(\chi) = 0$	$\cos m\phi = 0$ $\sin m\phi = 0$	$\sin k_z z = 0$ $\sin k_z z = 0$
nodal surfaces			

\*Valid for  $n > 0, n_z > 0$ .

where  $q$  is a non-negative integer less than or equal to  $4m$ . Thus  $\cos m\phi = 0$  and  $\sin m\phi = 0$  correspond to  $q$  being odd or even, respectively.

The  $r$ -nodal force surfaces are cylinders with  $r$  coordinates given by

$$r/a = \chi/\pi\alpha_{mn}, \tag{33}$$

where  $\chi$  is a solution of one or more of the following expressions, depending on the mode:

$$J_1(\chi) = 0, \quad m = 0, \tag{34}$$

$$(m+1)J_{m+1}(\chi) - (m-1)J_{m-1}(\chi) = 0, \quad m > 0, \tag{35}$$

$$J_m''(\chi) - (2f_1/3f_2)(k/k_r)^2 J_m(\chi) = 0, \quad m > 0. \tag{36}$$

The allowable  $\chi$  solutions are those for which  $r/a < 1$ . The radial coordinates of the potential minima determined from Eqs. (34) and (35) depend on the mode quantum numbers  $m$  and  $n$ . On the other hand, solutions of Eq. (36) also depend on the chamber aspect ratio  $a/l_z$  and sample properties (i.e.,  $f_1$  and  $f_2$ ). The potential minima for a given cylindrical mode are obtained from the selection rules for the  $r, \phi$ , and  $z$ -nodal force surfaces given in Table V. The positioning features of representative axial, tangential, and oblique cylindrical modes are discussed below.

The acoustic positioning properties of the ( $00n_z$ ) cylindrical  $z$ -axial modes are identical to those of the rectangular chamber as shown in Fig. 1. The ( $0m0$ )  $r$ -axial modes only depend on the radial coordinate  $r$ . For these modes  $\bar{p}, \bar{U}$ , and  $\bar{F}$  are given by:

$$\bar{p}(\chi) = J_0(\chi)\cos\omega t, \tag{37}$$

$$\bar{U}(\chi) = (f_1/3)J_0^2(\chi) - (f_2/2)J_1^2(\chi), \tag{38}$$

and

$$\bar{F}_r(\chi) = \left\{ \left[ \left( \frac{2f_1}{3} \right) + \left( \frac{f_2}{2} \right) \right] J_0(\chi) - \left( \frac{f_2}{2} \right) J_2(\chi) \right\} J_1(\chi). \tag{39}$$

The dependence of these functions on  $\chi$  is shown in Fig. 5 for a rigid sphere. The critical points of the potential correspond to positions where  $\bar{F}_r = 0$ . The position and magnitude of the first five potential maxima and minima for a rigid sphere

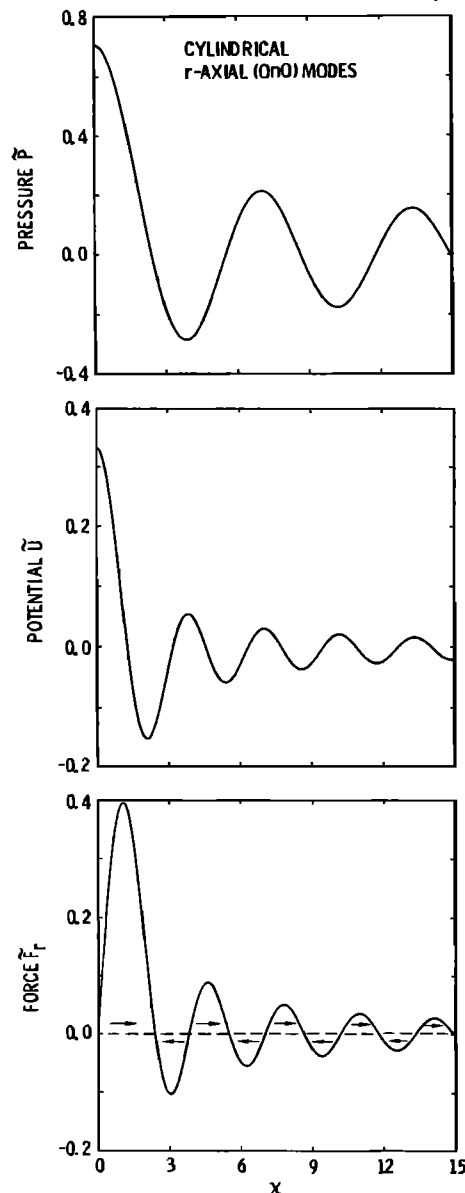


FIG. 5. Dependence of the acoustic pressure, potential, and force on the variable  $\chi = kr$ . As  $\chi$  increases, the depth of the potential wells and magnitude of the restoring forces decrease.

are given in Table VI. The potential maxima are given by the roots of  $J_1(\chi) = 0$ . Assuming  $f_1$  and  $f_2$  are positive, the magnitude of the potential is  $\tilde{U}_{\max} = (f_1/3)J_0^2(\chi)$ . The  $\chi = 0$  root of  $J_1$  corresponds to the cylindrical axis and yields the largest value of  $\tilde{U}_{\max}$ . Altogether there are  $n + 1$  maxima located at positions  $r/a = 0, (\alpha_{01}/\alpha_{0n}), \dots, (\alpha_{0n-1}/\alpha_{0n}), 1$ . The potential minima correspond to the zeros of the term in braces in Eq. (39) and are situated between positions of successive maxima. There are  $n$  minima, all in the interior of the chamber. The depth of the potential wells decreases as  $\chi$  (or  $r/a$ ) increases. The potential maxima and minima for the  $r$ -axial modes are nonisolated critical points. They are cylindrical surfaces concentric to the cylindrical axis and extending between the  $z/l_z = 0$  and  $1$  chamber walls.

In Fig. 6, we show the dimensionless quantities  $\tilde{p}$ ,  $\tilde{U}$ , and  $\tilde{F}_r$  as functions of  $r/a$  for the lowest order (010)  $r$ -axial cylindrical mode. The potential minimum cylindrical surface occurs at  $r/a = 0.551$ . This minimum does not coincide with the acoustic pressure nodal surface ( $r/a = 0.628$ ) in contrast to the case of axial modes in a rectangular chamber. This difference is due to the fact that the  $r$ -axial nodal cylindrical surface depends on the chamber aspect ratio and sample properties. The potential well for the (010) mode is asymmetric, resulting in a stronger outward-going restoring force. As was the case with the  $z$ -axial modes, the  $r$ -axial modes by themselves cannot produce a unique equilibrium localization position.

The  $(mn0)$   $\phi$ ,  $r$ -tangential modes have strikingly different acoustic behavior than the  $r$ -axial modes due to the finite value of the quantum number  $m$  which introduces a  $\phi$  dependence. The potential minimum surfaces for these modes may be visualized from the intersection of nodal force  $r$  cylinders and  $\phi$  planes which produce potential minima lines. These  $(mn0)$  modes have two sets of nonisolated potential minima lines. The set defined by the  $r$  coordinate solutions of Eq. (35) are situated at angles  $\phi$  given by  $\cos m\phi = 0$ , while those corresponding to Eq. (36) are at  $\phi$  values satisfying  $\sin m\phi = 0$ . For each unit increase in  $n$  there are  $4m$  new lines introduced into the cylinder. The  $m = 1$  modes are the most interesting for application purposes. For these  $m = 1$  modes, one set of  $r$ -nodal force surfaces [Eq. (35)] requires  $J_2(\chi) = 0$ . The lowest-order solution gives  $r/a = 0$  which can be thought of as the shrinking of an  $r$ -nodal force cylinder into the axial line. These  $(1n0)$  modes have a potential minimum  $\tilde{U}_{\min} = -f_2/8$  along the cylindrical axis. To illustrate the behavior of these modes, the radial dependence of  $\tilde{p}$ ,  $\tilde{U}$ ,

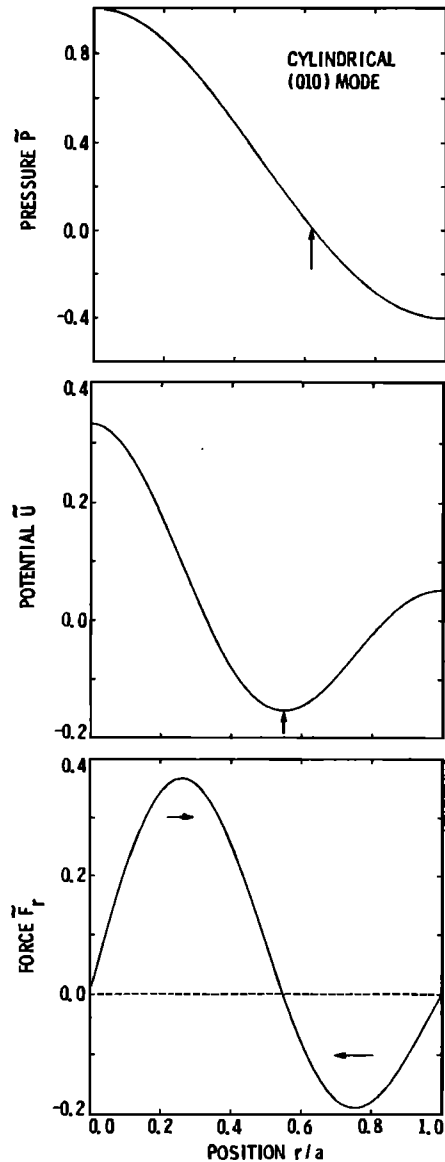


FIG. 6. Radial dependence of the acoustic pressure, potential, and force for the (010)  $r$ -axial cylindrical mode. The position of the nonisolated cylindrical potential minimum does not coincide with the pressure nodal cylinder. The restoring force is asymmetric with the outward-going force being the strongest.

TABLE VI. Position and magnitude of the first five force potential maxima and minima of the  $(0n0)$   $r$ -axial cylindrical modes for a rigid sphere.

$\chi_{\max}^*$	$\tilde{U}_{\max}$	$\chi_{\min}^*$	$\tilde{U}_{\min}$
0.0	0.3333	2.109	-0.1522
3.832	0.0541	5.408	-0.0591
7.016	0.0300	8.564	-0.0371
10.173	0.0208	11.740	-0.0271
13.324	0.0159	14.891	-0.0214

\*The radial position of a maximum or minimum is determined using  $r/a = \chi/\pi\alpha_{0n}$ .

and  $\tilde{F}_r$  for a rigid sphere is shown in Fig. 7 for the (100) tangential mode. The solid and dashed lines correspond to  $\phi = 0$  and  $\pi/2$ , respectively. The height of the potential well is largest along the direction  $\phi = 0$  ( $\pi$ ) and decreases to its smallest value for  $\phi = \pi/2$  ( $3\pi/2$ ). The maximum restoring force occurs at  $r/a = 0.493$  for  $\phi = 0$  ( $\pi$ ). While the radial acoustic force is weakest along the directions  $\phi = \pi/2$  ( $3\pi/2$ ), it has a finite restoring force at the chamber wall,  $r/a = 1$ . This finite force component at the wall directed toward the interior is a feature of cylindrical geometry that is not shared by rectangular chamber modes where the normal force components at the walls are always zero.

Only the  $m = 1$ ,  $(1n0)$  modes have a potential minimum line along the axis ( $r/a = 0$ ). All other minima lines for  $m > 1$  occur at finite  $r$  values. The positions of these minima lines are illustrated in Fig. 8 where we present a  $\phi$ ,  $r$ -contour graph of the radiation potential for the (210) cylindrical



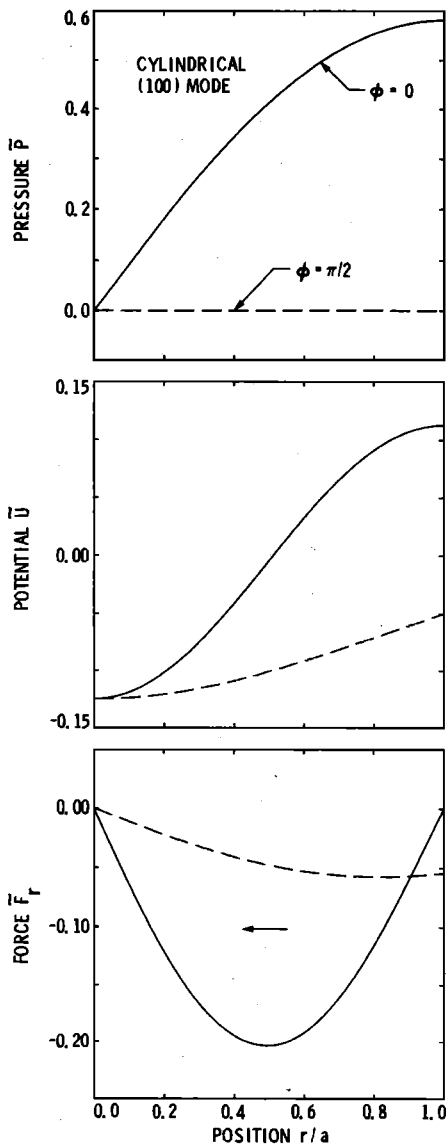


FIG. 7. Radial dependence of the acoustic pressure, potential, and force for the (100)  $\phi, r$ -tangential cylindrical mode. The potential minimum is a nonisolated line along the axis of the cylinder. The restoring force is finite at the chamber walls except for  $\phi = 0, \pi$ .

mode. For this mode there is a potential maximum at  $r/a = 0$  and 12 minima lines, four each on three radial circles. The radii of the inner and outer circles correspond to solutions of Eq. (35) while the middle circle radius is a solution of Eq. (36).

The  $(0nn_z)$   $r, z$ -tangential modes differ from the  $\phi, r$ -tangential modes in that the  $\phi$  dependence has been replaced by a  $z$  dependence. Now, since  $m = 0$ , the intersection of the nodal force  $r$  cylinders and the  $z$  planes leads to nonisolated potential minima circles and to isolated potential minima points. Again, there are two sets of potential minima with radii defined by either Eq. (34) or Eq. (36). All solutions to Eq. (36) give nonzero radii. This set always includes circles at the  $z$  walls,  $z/l_z = 0$  or 1. The  $r$ -coordinate solutions to Eq. (34) also include the axis  $r/a = 0$ . Thus this second set includes isolated potential minima points along the axis as well as nonisolated circles located at positions  $r/a = (\alpha_{01}/\alpha_{0n}), \dots, (\alpha_{0n-1}/\alpha_{0n}), 1$ . This second set always has circles at the  $r/a = 1$  walls. These potential minima are

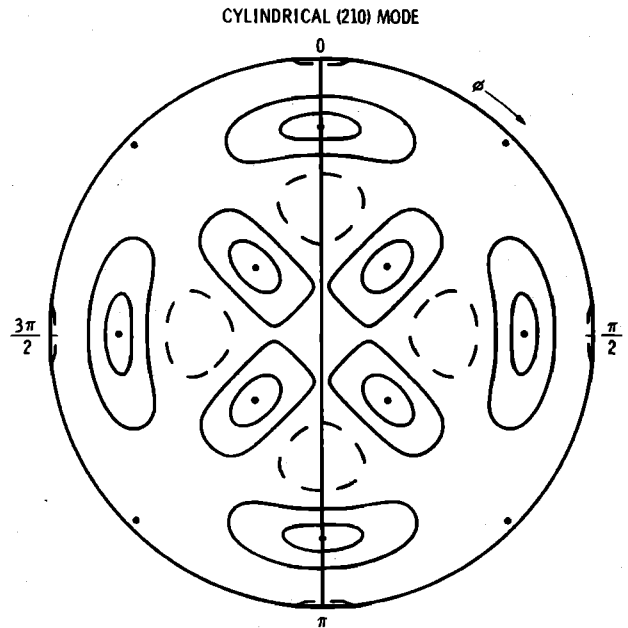


FIG. 8.  $\phi, r$ -contour graph of the acoustic potential for the (210)  $\phi, r$ -tangential cylindrical mode. There are 12 nonisolated potential minima lines situated in sets of four on three radial circles.

shown in Fig. 9, which represents a hidden line graph of the (011) mode potential. In the  $z/l_z = 0.5$  midplane, this mode has a minimum point at the chamber center  $r/a = 0$  and a minimum circle at the  $r/a = 1$  wall. In addition, there are another two minima circles at  $r/a = 0.605$ , one on each  $z$  wall ( $z/l_z = 0$  and 1). The  $(0nn_z)$  modes have  $n_z$  interior minimum points along the axis at positions  $z/l_z = m_z/2n_z$  with  $m_z = 1, 3, \dots, 2n_z - 1$ .

The potential minima of the  $(mnn_z)$  oblique cylindrical modes are all isolated points since they are determined from the intersection of three orthogonal nodal force surfaces ( $\phi, r$ , and  $z$ ). These minima points may also be derived from the properties of the axial and tangential modes. For example, let us first compare the potential minima of the (100)  $\phi, r$ -tangential mode shown in Fig. 7 and the  $(10n_z)$  oblique

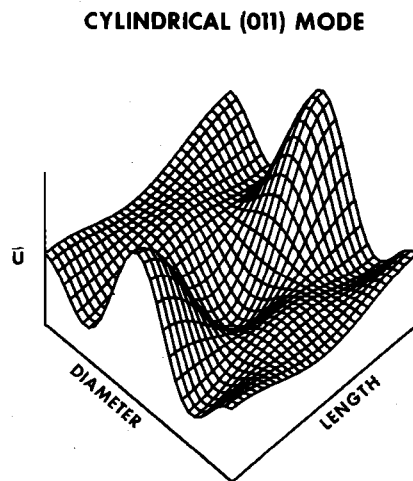


FIG. 9. Hidden line graph of the acoustic potential for the (011) cylindrical mode. This mode has no  $\phi$  dependence. There is an isolated minimum point at the chamber center and three nonisolated minima circles, two on the  $z$  walls and one on the cylinder wall in the midplane  $z/l_z = 0.5$ .

CYLINDRICAL (102) MODE

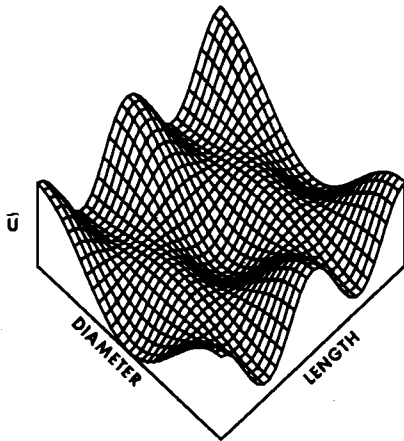


FIG. 10. Hidden line graph of the acoustic potential for the (102) cylindrical mode in the  $\phi = 0$  plane. There is an isolated minimum point at the chamber center and six minima points on the walls.

modes. The introduction of the  $z$  dependence in the  $(10n_z)$  oblique modes leads to a preferential selection of  $n_z + 1$  specific minima points from the infinite number of such points along the potential minimum line  $r/a = 0$  of the (100) mode. The  $z$  coordinates of these minima along the axis are given by Eq. (18) with  $m_z$  even. Thus the (101) mode has two potential minima, one at each  $z$  wall. The lowest oblique mode to have an isolated potential minimum point in the chamber interior is the (102) mode. A hidden line graph of the (102) mode potential is shown in Fig. 10. This mode has isolated potential minima at the chamber center ( $r/a = 0, a/l_z = 0.5$ ) and at the center ( $r/a = 0$ ) of each  $z$  wall ( $z/l_z = 0$  and 1). In general, the  $(10n_z)$  modes have  $n_z - 1$  interior isolated minima along the axis at positions  $z/l_z = m_z/2n_z$  with  $m_z = 2, 4, \dots, 2n_z - 2$ .

Extending this comparison to any  $(mnn_z)$  mode shows that increasing  $m$  by 1 introduces two additional  $\phi$ -nodal

force planes that can intersect the existing  $r$ - and  $z$ -nodal force surfaces to produce new potential minima. Similarly, increasing  $n$  by 1 introduces an additional  $r$ -nodal force cylinder into the chamber. The characteristics of the potential minima for the various cylindrical modes discussed in Sec. III are given in Table VII.

IV. SPHERICAL GEOMETRY

In a spherical chamber of radius  $r_0$ , a spatial position is designated by the  $\theta, r$ , and  $\phi$  coordinates ( $\theta r \phi$ ) and a normal mode is given by the quantum numbers  $l, n$ , and  $m, (lnm)$ .<sup>20</sup> The origin (000) for the spherical coordinate system is chosen to be at the chamber center. The sphere is the most symmetric of the three geometries discussed in this paper and has positioning features not found in rectangular and cylindrical geometries.

The velocity potential for a standing wave field in a spherical chamber is given by<sup>23,24</sup>

$$\Phi_{in} = - (v_0/k_{in}) j_l(\xi) P_l^m(\mu) \cos m\phi \sin \omega t, \quad (40)$$

where  $\xi = k_{in} r$  and  $\mu = \cos \theta$  with

$$k_{in} = \omega/c = \pi \gamma_{in}/r_0. \quad (41)$$

Assuming rigid boundary conditions,  $\gamma_{in}$  is a solution of the relation  $d [j_l(\pi \gamma)]/d\gamma = 0$ , where  $j_l$  is the spherical Bessel function of order  $l$ . Using Eq. (1), we obtain the following dimensionless radiation potential for the  $(lnm)$  normal mode:

$$\begin{aligned} \tilde{U} = & (f_1/3) j_l^2(\xi) [P_l^m(\mu)]^2 \cos^2 m\phi - (f_2/2) ([j_l(\xi)/\xi \\ & - j_{l+1}(\xi)]^2 [P_l^m(\mu)]^2 \cos^2 m\phi \\ & + \{ [j_l(\xi)/\xi ]^2 / (1 - \mu^2) \} \{ [(l+1)\mu P_l^m(\mu) \\ & - (l-m+1)P_{l+1}^m(\mu)]^2 \cos^2 m\phi \\ & + [mP_l^m(\mu)]^2 \sin^2 m\phi \}. \end{aligned} \quad (42)$$

The dimensionless force components for a spherical chamber are obtained using the following expressions:




TABLE VII. Characteristics of potential minima for a rigid sphere for various modes in cylindrical geometry.

Mode	Surface	Location	Number of minima
$z$ axial ( $00n_z$ )	plane	interior and $r$ wall	$n_z$
$r$ axial ( $0n0$ )	cylindrical	interior and $z$ walls	$n$
$\phi, r$ tangential <sup>a</sup> ( $mnn_0$ )	line	interior and $z$ walls	$2m(2n+1) - \delta_{m1}$
$r, z$ tangential ( $0nn_z$ )	point	interior	$n_z$
	interior	interior	$2nn_z - n - n_z$
	circle	$z$ walls	$2n$
oblique <sup>b</sup> ( $mnn_z$ )	point	$r$ wall	$n_z$
		interior	$2m[(3n+1 - \delta_{m1})n_z - (2n+1 - \delta_{m1})]$
		$z$ walls	$4m(2n+1) - 2\delta_{m1}$
		$r$ wall	$2mn_z$

<sup>a</sup> Includes  $(m00)$  modes.

<sup>b</sup> Includes  $(m0n_z)$  modes.

TABLE VIII. Potential minima nodal force surfaces for various modes in spherical geometry.

Mode	$r$	$\phi$	$\theta$
	$j_{l+1}(\xi) - (\xi/2)[2f_1/3f_2 + 1 - l(l-1)/\xi^2]j_l(\xi) = 0$	$\sin m\phi = 0$	$(l-m+1)P_{l+1}^m(\mu) - (l+1)\mu P_l^m(\mu) = 0$
all modes ( $lmn$ )	$\xi j_{l+1}(\xi) - (l-1)j_l(\xi) = 0$	$\sin m\phi = 0$ $\cos m\phi = 0$	$\mu = 0$ $(l-m+1)P_{l+1}^m(\mu) - (l+2)\mu P_l^m(\mu) = 0$ $\mu = \pm 1$
nodal surfaces	 sphere	 plane	 cone

$$\tilde{F}_r = -\frac{\partial \tilde{U}}{\partial \xi}, \tag{43}$$

$$\tilde{F}_\theta = -\xi^{-1} \left( \frac{\partial \tilde{U}}{\partial \theta} \right), \tag{44}$$

$$\tilde{F}_\phi = -(\xi \sin \theta)^{-1} \frac{\partial \tilde{U}}{\partial \phi}. \tag{45}$$

Explicit expressions for these force components are given in Appendix C. For discussion purposes, the normal modes of a spherical chamber will be divided into  $r$ -axial,  $\theta$ ,  $r$ -tangential, and oblique modes. The  $(0n0)$   $r$ -axial modes have only radial motion while the  $(ln0)$   $\theta$ ,  $r$ -tangential modes have motion in the  $r$  and  $\theta$  directions only (no  $\phi$  dependence).

As was the case for rectangular and cylindrical geometries, the potential minima for spherical modes can be obtained from the intersection of sets of  $r$ -,  $\theta$ -, and  $\phi$ -nodal force surfaces.<sup>24</sup> The types of nodal force surfaces for spherical geometry are shown at the bottom of Table VIII. In the case of spherical modes, the  $\phi$ -constant nodal force surfaces are circular half-planes with coordinate positions given by Eq. (32). The  $\theta$ -constant nodal force surfaces are cones with  $\theta$  coordinates given by

$$\theta = \cos^{-1} \mu, \tag{46}$$

where  $\mu$  is a solution of one or more of the following expressions:

$$\mu = 0, \pm 1, \tag{47}$$

$$(l-m+1)P_{l+1}^m(\mu) - (l+1)\mu P_l^m(\mu) = 0, \tag{48}$$

$$(l-m+1)P_{l+1}^m(\mu) - (l+2)\mu P_l^m(\mu) = 0. \tag{49}$$

The  $r$ -constant nodal force surfaces are spheres with  $r$  coordinates given by

$$r/r_0 = \xi / \pi \gamma_{ln}, \tag{50}$$

where  $\xi$  is a solution of one or more of the following expressions, depending on the mode:

$$\xi j_{l+1}(\xi) - (l-1)j_l(\xi) = 0, \tag{51}$$

$$j_{l+1}(\xi) - (\xi/2)[2f_1/3f_2 + 1 - l(l-1)/\xi^2]j_l(\xi) = 0. \tag{52}$$

The allowable  $\xi$  solutions are those for which  $r/r_0 < 1$ . Solutions to Eq. (51) depend on the mode quantum numbers, while solutions to Eq. (52) also depend on sample properties through  $f_1$  and  $f_2$ . This dependence of the position of a potential minimum on the properties of the sample was also observed in cylindrical geometry but not in rectangular geometry.

try. Table VIII gives the selection rules for determining the sets of  $r$ -,  $\theta$ -, and  $\phi$ -nodal force surfaces corresponding to potential minima obtained from the closed form expressions [Eq. (32) and Eqs. (46)–(52)]. Besides the selection rules presented in Table VIII, there is an additional set with the  $\phi$ -nodal force surface satisfying  $\sin m\phi = 0$ . However, closed form expressions for the  $r$ - and  $\theta$ -nodal force surfaces for this set cannot be obtained since the  $r$  and  $\theta$  dependences do not decouple in the force expressions, Eqs. (43) and (44).

The positioning features of representative axial, tangential, and oblique spherical modes are discussed below. The  $(0n0)$   $r$ -axial modes are independent of  $\theta$  and  $\phi$ . For these modes, the dimensionless parameters  $\tilde{p}$ ,  $\tilde{U}$ , and  $\tilde{F}$ , are

$$\tilde{p}(\xi) = j_0(\xi) \cos \omega t, \tag{53}$$

$$\tilde{U}(\xi) = (f_1/3)j_0^2(\xi) - (f_2/2)j_1^2(\xi), \tag{54}$$

$$\tilde{F}_r(\xi) = \{ [(2f_1/3f_2) + 1] j_0(\xi) - (2/\xi) j_1(\xi) \} f_2 j_1(\xi). \tag{55}$$

These parameters have a decaying oscillatory dependence on  $\xi$  similar to the  $r$ -axial cylindrical mode dependencies on  $\chi$  shown in Fig. 5. The position and magnitude of the first five potential maxima and minima for a rigid sphere are given in Table IX. The positions of the potential maxima correspond to the roots of  $j_1(\xi) = 0$  [see Eq. (55)], and assuming  $f_1$  and  $f_2$  positive, the potential has a magnitude given by  $\tilde{U}_{\max} = (f_1/3)j_0^2(\xi_{\max})$ . The lowest root  $\xi_{\max} = 0$  corresponds to the center of the sphere and yields the largest value of  $\tilde{U}_{\max}$ . For a given  $(0n0)$  mode, there are  $n+1$  maximum spherical surfaces at  $r/r_0 = 0, \gamma_{01}/\gamma_{0n}, \dots, \gamma_{0n-1}/\gamma_{0n}, 1$ . The potential minima are obtained from the zero of the term in braces in Eq. (55) and are situated between positions of successive maxima. Altogether there are  $n$  minima, all in the chamber

TABLE IX. Position and magnitude of the first five force potential maxima and minima of the  $(0n0)$   $r$ -axial spherical modes for a rigid sphere.

$\xi_{\max}^a$	$\tilde{U}_{\max}$	$\xi_{\min}^a$	$\tilde{U}_{\min}$
0.0	0.33333	2.639	-0.06939
4.493	0.01573	6.082	-0.01350
7.725	0.00550	9.295	-0.005787
10.904	0.00278	12.470	-0.003215
14.066	0.00157	15.631	-0.002046

<sup>a</sup>The radial position of a maximum or minimum is determined using  $r/r_0 = \xi / \pi \gamma_{0n}$ .

interior. These potential maxima and minima are concentric spherical surfaces and, except for the origin  $r/r_0 = 0$ , they are nonisolated critical points. The potential maximum at the origin may be thought of as a sphere that has collapsed to an (isolated) point.

The dimensionless parameters  $\bar{p}$ ,  $\bar{U}$ , and  $\bar{F}_r$ , are shown in Fig. 11 as a function of  $r/r_0$  for the lowest-order  $r$ -axial spherical mode (010). The  $r$ -axial spherical and cylindrical modes have similar features (see Fig. 6). The potential minimum spherical surface occurs at  $r/r_0 = 0.587$  and has a radius less than the pressure nodal sphere ( $r/r_0 = 0.699$ ). There is greater asymmetry in the spherical potential well than the cylindrical well which leads to an even stronger outward-going force.

The  $(ln0) \theta, r$ -tangential modes are the most interesting for application purposes. Since there is no  $\phi$  dependence ( $m = 0$ ) for these modes, the potential minima correspond to

the intersection of  $r$ -spherical and  $\theta$ -conical nodal force surfaces. In general, these intersections are circles. However, there are two special cases that lead to isolated potential minima. For  $l = 1$ , one set of  $r$ -nodal force surfaces [Eq. (51)] requires  $j_2(\xi) = 0$ . The lowest-order solution gives  $r/r_0 = 0$  which corresponds to an isolated potential minimum in the center of the sphere. This shrinking of the radial nodal force sphere to the origin only occurs for the  $l = 1$  modes. To illustrate this special case, the radial dependence of the dimensionless parameters  $\bar{p}$ ,  $\bar{U}$ , and  $\bar{F}_r$ , is shown in Fig. 12 for the (100)  $\theta, r$ -tangential mode. The radial dependence of these parameters for  $\theta = 0$  and  $\pi/2$  are very similar to the behavior of the (100)  $\phi, r$ -tangential cylindrical mode for  $\phi = 0$  and  $\pi/2$  (see Fig. 7). The maximum restoring force occurs at  $r/r_0 = 0.487$  for  $\theta = 0$ . There is a finite restoring force at the chamber wall,  $r/r_0 = 1$  for all  $\theta$  values differing from 0 or  $\pi$ .

For finite  $n$  values, a second set of isolated potential

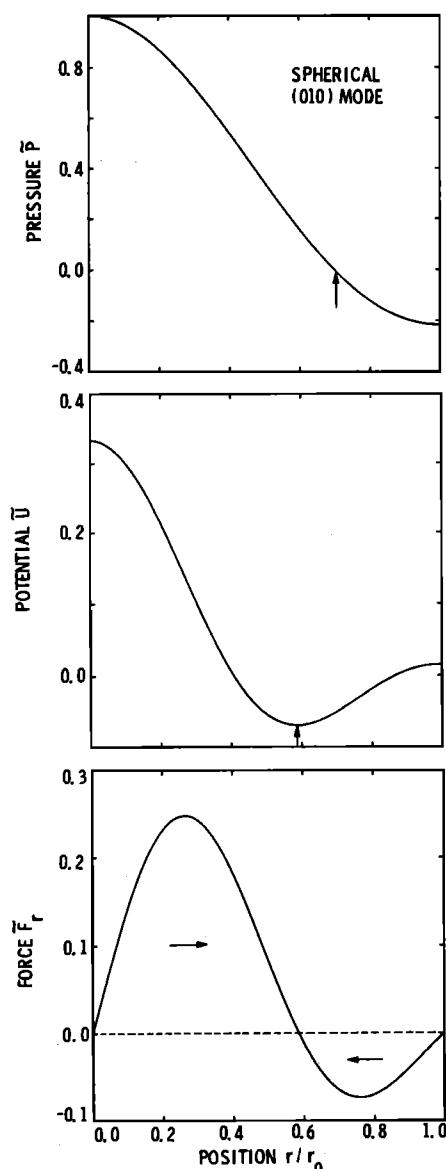


FIG. 11. Radial dependence of the acoustic pressure, potential, and force for the (010)  $r$ -axial spherical mode. The potential minimum is a nonisolated spherical surface that does not coincide with the pressure nodal sphere. The outward-going restoring force is much stronger than the inward-going force. The mode has similar features to the (010)  $r$ -axial cylindrical mode.

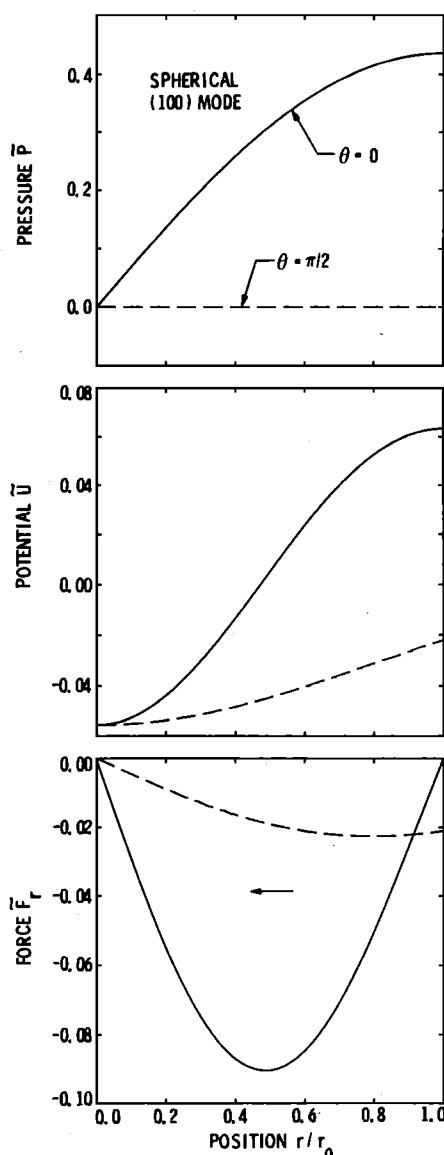


FIG. 12. Radial dependence of the acoustic pressure, potential, and force for the (100)  $\theta, r$ -tangential spherical mode. This mode has an isolated potential minimum point at the chamber center. The restoring force near the minimum is strongest along the  $\theta = 0$  direction. The restoring force is finite at the chamber walls except for  $\theta = 0, \pi$ .

minima occurs for the  $(ln0)$  modes. These unique points arise from the shrinking of the  $\theta$ -nodal force cones into the lines  $\theta = 0, \pi$ . There are  $2n$  potential minima for this set with  $n$  positions along each of the lines  $\theta = 0$  and  $\pi$  at the same  $r/r_0$  values determined from Eq. (51).

The wavelength and resonance frequency of a spherical mode are specified by the  $l$  and  $n$  quantum numbers [see Eq. (41)]. For spherical modes, there are  $2l + 1$  degenerate modes for each quantum number  $l$ . These degenerate modes are specified by the quantum number  $m$  which has integer values between  $-l$  and  $l$ . Different  $m$  values lead to different spatial distributions of the dimensionless parameters  $\bar{p}$ ,  $\bar{U}$ , and  $\bar{F}$ . The axial and tangential spherical modes discussed above have  $m = 0$  and are independent of  $\phi$ . The  $(lnm)$  oblique spherical modes are distinguished by finite  $m$  values ( $|m| < l$ ) that give these modes a  $\phi$  dependence. The radiation potential and forces for negative  $m$  values are simply related to those of positive  $m$  values through the expressions,

$$\bar{U}(-m) = (C_l^m)^2 \bar{U}(m), \quad (56)$$

$$\bar{F}_i(-m) = (C_l^m)^2 \bar{F}_i(m), \quad (57)$$

where

$$C_l^m = (-1)^m (l - m)! / (l + m)!. \quad (58)$$

For finite  $m$ ,  $C_l^m < 1$  and decreases with increasing  $m$ . Thus the negative  $m$  modes produce much weaker acoustic potential wells and restoring forces. Since the only difference between the acoustic properties of positive and negative  $m$  values is in the scale, evaluation of either positive or negative  $m$  modes will define the positions of the potential minima. In the rest of Sec. IV, we will consider only positive  $m$  modes.

We carried out a detailed analysis of the potential minima positions for the oblique spherical modes with  $l < 2$ . All of these modes have  $2ln$  minima points along the  $\theta = 0, \pi$  lines independent of  $m$ . Various additional combinations of potential minima given by the selection rules in Table VIII appear as  $l$  and  $m$  increase.

In general, the potential minima of oblique spherical modes are isolated critical points derived from the intersection of  $r$ -,  $\theta$ -, and  $\phi$ -nodal force surfaces. However, the high degree of symmetry in the spherical geometry can lead to a situation where only two of the variables need to be specified in order to have all the forces vanish. This case occurs only for the  $(1n1)$  modes where, for one potential minima set, the  $\phi$ -nodal force surfaces satisfy  $\phi = \pi/2, 3\pi/2$  and the  $r$ -nodal force surfaces satisfy Eq. (51). For these  $\phi$  values, the force  $F_\phi = 0$  for all  $r$  and  $\theta$ . This unique circumstance leads to  $n$  potential minima circles in the  $\phi = \pi/2, 3\pi/2$  plane. The characteristics of the potential minima for the various spherical modes discussed in Sec. IV are given in Table X.

## V. DISCUSSION

It is of interest to compare the positioning capabilities of various modes in the same geometry as well as in different geometries. Let us initially assume the same sample and gas medium is used in these comparisons. Then, for dimensioned variables

$$\left(\frac{F_{1i}}{F_{2j}}\right) = \left(\frac{v_{10}}{v_{20}}\right)^2 \left(\frac{k_1}{k_2}\right)^2 \left(\frac{\bar{k}_{1i}}{\bar{k}_{2j}}\right) \left(\frac{l_{1i}}{l_{2j}}\right) \left(\frac{x_{1i}}{l_{1i}} / \frac{x_{2j}}{l_{2j}}\right), \quad (59)$$

TABLE X. Characteristics of potential minima for a sphere for various modes in spherical geometry.

Mode	Surface	Location	Number of minima*
$r$ axial (0n0)	sphere	interior	$n$
$\theta, r$ tangential (ln0)	point	interior	$2n + \delta_{l1}$
	circle	interior	$n + 2(n + 1)(1 - \delta_{l1})$
oblique (lnm)	point	interior	$2ln + \delta_{l1}$ $+ (l - \delta_{l1})(n + 1)(m + 1)$
oblique (1n1)	circle	interior	$n$

\* Valid for  $l < 2$ .

where the modes 1 and 2 can be the same mode, different modes in the same geometry, or modes of different geometries. The subscripts  $i$  and  $j$  describe the dimensioned variable of interest in modes 1 and 2, respectively. In this discussion we will compare restoring forces at the same relative displacement,  $x_i/l_i < 1$ , from the equilibrium position. For comparison of modes in different geometries, it is usually convenient to specify certain additional constraints. The modes may be required to have the same resonance frequency, maximum particle velocity, average energy density, chamber volume, or some combination of these or other constraints.

As an example, let us consider the  $x, y$ , and  $z$  restoring forces for the (221) rectangular mode in a resonator of square cross section ( $l_x = l_y$ ). The restoring force constants are

$$\bar{k}_x = f_2 k_x^2 k_z^2 / k^4, \quad \bar{k}_y = f_2 k_y^2 k_z^2 / k^4, \quad (60a)$$

$$\bar{k}_z = \left(\frac{k_z}{k}\right)^2 \left[ \frac{2f_1}{3} + f_2 \left(\frac{k_z}{k}\right)^2 \right], \quad (60b)$$

and the ratio of  $F_x$  to  $F_z$  at the same relative displacement is

$$\frac{F_x}{F_z} = 4 \left(\frac{l_z}{l_x}\right) \left[ \left(\frac{16f_1}{3f_2}\right) \left(\frac{l_z}{l_x}\right)^2 + \frac{2f_1}{3f_2} + 1 \right]^{-1}. \quad (61)$$

For a rigid sphere  $F_x/F_z < 1$  with the largest value of this ratio being 0.67 for  $l_z/l_x = 0.55$ . The ratio  $F_y/F_z$  has the same form as Eq. (61) with  $x$  replaced by  $y$ . Thus  $F_z$  will always be larger than  $F_x = F_y$ .

We will now compare the lowest-order single mode positioners in each geometry, e.g., the (221) rectangular mode, the (011) cylindrical mode, and the (100) spherical mode. It will be assumed that each resonator has the same volume and the same maximum particle velocity. For each mode there is a particular direction that has the weakest restoring force. This direction is determined by comparing the orthogonal dimensioned force components associated with translational stability. The  $\bar{F}_\theta$  and  $\bar{F}_\phi$  dimensionless forces are associated with rotational stability and will not be considered here. Except for spherical geometries, the strength of the weakest force component can be maximized by the appropriate adjustment of the chamber dimension ratios. The various restoring force components will be compared for the same

relative displacement,  $x_i/l_i \ll 1$ , from the equilibrium position.

In the (221) rectangular mode, the force in the  $z$  direction is always larger than the  $x$  and  $y$  force components, as shown above. For a given dimension  $l_z$ , the  $x$  and  $y$  forces will be maximum and equal when the length ratio  $l_y/l_x = 1$ . For a constant volume constraint, these  $x$  and  $y$  forces are further maximized by having  $l_x/l_z = 2\sqrt{10}$ . For these dimension ratios, the  $x$  and  $y$  restoring forces are approximately a third of the  $z$  restoring force.

For the (011) cylindrical mode, the  $z$  force component is again always larger than the radial force. The weaker radial force is maximized for the dimension ratio  $a/l_z = \sqrt{5}\alpha_{01}$ . The radial restoring force is about six and a half times weaker than the  $z$  restoring force for this dimension ratio.

The (100) spherical mode has a radial restoring force that depends on the angle  $\theta$ . The maximum restoring force is along  $\theta = 0$  and is approximately six and a half times stronger than the weakest direction  $\theta = \pi/2$ . Maximization of the restoring forces with respect to chamber dimensions is not possible in a sphere for the assumption of a constant volume resonator. For the imposed constraints, this analysis shows that the (221) rectangular mode has the strongest restoring forces. The ratio of the weakest restoring forces between each mode are (221) rectangular/(011) cylindrical = 2.8 and (221) rectangular/(100) spherical = 115. If, instead of having the same maximum particle velocity  $v_0$  in each geometry, we assume the same space-time-averaged energy density  $\langle \bar{\epsilon} \rangle$  (see Appendix D), we find the following ratios for the weakest restoring forces: (221) rectangular/(011) cylindrical = 1.65 and (221) rectangular/(100) spherical = 47. These comparisons suggest that the overall positioning ability of the single mode levitators decreases as the chamber symmetry increases. This is partially due to the fact that the optimization of the chamber dimension ratios becomes more limiting with increased symmetry.

The expressions developed in this paper were analyzed primarily for a rigid sphere. However, these expressions are also applicable to the general case of samples with arbitrary density and compressibility. Of particular interest in this regard is the acoustic behavior of gas bubbles in a liquid. Resonators with free boundaries is another area where the analysis is useful. The only required change in the analysis is the use of different boundary condition coefficients (i.e.,  $n_i$ ,  $\alpha_{mn}$ , or  $\gamma_n$ ).

A useful feature of Gor'kov's<sup>9</sup> method is the ability to couple the acoustic force field with other external fields such as gravity. Under these conditions, the resultant force field is simply determined by summing the force potentials and taking the appropriate derivatives. This procedure will lead to new potential minima positions and restoring force constants. An investigation of the effect of gravity on acoustically positioned samples in arbitrarily oriented chambers is now in progress.

## VI. CONCLUSIONS

In this paper, we have developed expressions for the acoustic radiation potential and forces in rectangular, cylindrical, and spherical geometries. The critical points were

analyzed to determine the positions of potential minima which correspond to unique localization positions. Besides isolated potential minima points, nonisolated minima consisting of lines and circles, and plane, cylindrical, and spherical surfaces were also obtained. It was demonstrated in cylindrical and spherical geometries that under special conditions certain tangential modes are capable of producing isolated potential minima. Conversely, certain oblique spherical modes exhibit nonisolated potential minima circles.

This analysis has demonstrated that in each geometry there are single acoustic modes that can position a small sample at the center of the chamber. The lowest-order modes in each geometry that exhibit isolated potential minima are the (221), (212), and (122) modes in rectangular geometries, the (011) and (102) modes in cylindrical geometries, and the (100) mode in spherical geometries. Stable positioning of small samples was demonstrated experimentally for all of these modes.<sup>25</sup> Isolated potential minima may also be produced by the simultaneous excitation of two or more modes, each of which individually cannot produce isolated minima. The most practical set of modes that can position a sample at the chamber center are the (102) and (010) rectangular modes and the (100) and (001) cylindrical modes. The present investigation has presented acoustic positioning properties of various modes in different geometries that will have application in basic and applied research programs.

## ACKNOWLEDGMENTS

We thank Dr. Carl Shipley and H. Jordan Brown for programming support. We also appreciate the careful reading of the manuscript by James L. Allen and the perseverance and patience of Sandi Thomas in typing the manuscript.

## APPENDIX A: CRITICAL POINTS OF A FUNCTION OF SEVERAL VARIABLES

We give below a brief summary (without proofs) of the results and terminology pertinent to this paper, concerning the critical points of a function  $f$  of several variables:  $x_1, x_2, \dots, x_n$ . For our cases  $n$  is at most 3. We assume that  $f_1(x_1, \dots, x_n)$  is differentiable as many times as necessary.

A point  $x_c = (x_{1c}, x_{2c}, \dots, x_{nc})$  is a *critical point* of  $f$  if

$$\left. \frac{\partial f}{\partial x_1} \right|_{x_c} = \left. \frac{\partial f}{\partial x_2} \right|_{x_c} = \dots = \left. \frac{\partial f}{\partial x_n} \right|_{x_c} = 0. \quad (\text{A1})$$

The value of  $f(x_c)$  at a critical point  $x_c$  is called the *critical value* of  $f$ .

In order to determine the type of critical point at  $x_c$ , we form the so-called *Hessian matrix* of  $f$ . The Hessian of  $f$ , denoted by  $Hf$ , is the symmetric matrix of all possible second partial derivatives of  $f$ , i.e.,

$$Hf = \begin{pmatrix} \frac{\partial^2 f}{\partial x_1^2} & \frac{\partial^2 f}{\partial x_1 \partial x_2} & \dots & \frac{\partial^2 f}{\partial x_1 \partial x_n} \\ \frac{\partial^2 f}{\partial x_2 \partial x_1} & \frac{\partial^2 f}{\partial x_2^2} & \dots & \frac{\partial^2 f}{\partial x_2 \partial x_n} \\ \vdots & \vdots & \ddots & \vdots \\ \frac{\partial^2 f}{\partial x_n \partial x_1} & \frac{\partial^2 f}{\partial x_n \partial x_2} & \dots & \frac{\partial^2 f}{\partial x_n^2} \end{pmatrix}. \quad (\text{A2})$$

The Hessian is diagonalizable and its eigenvalues may be found by the usual techniques. The determinant of the matrix  $Hf|_{x_c}$ , denoted  $\det(Hf|_{x_c})$ , and the trace of  $Hf|_{x_c}$ , denoted  $\text{tr}(Hf|_{x_c})$ , are invariant under the transformation which yields the eigenvalues  $\kappa_i$ . Thus we have

$$\det(Hf|_{x_c}) = \prod_{i=1}^n \kappa_i \quad (\text{A3})$$

and

$$\text{tr}(Hf|_{x_c}) = \sum_{i=1}^n \kappa_i. \quad (\text{A4})$$

We also wish to remind the reader of two useful terms: The rank  $r$  of an  $n \times n$  matrix is the order of the largest submatrix with a nonvanishing determinant, while the corank  $m = n - r$ . Clearly then, the rank is equal to the number of nonzero eigenvalues, while the corank is equal to the number of eigenvalues which are equal to zero.

The type of critical point at  $x_c$  is determined from a consideration of the various possibilities listed below:

(1) All the eigenvalues of  $Hf|_{x_c}$  are different from zero [i.e.,  $\det(Hf|_{x_c}) \neq 0, r = n, m = 0$ ]. In this case we have a nondegenerate critical point. It can be shown that a nondegenerate critical point of  $f$  is an isolated critical point of  $f$ ; i.e., there are no other critical points within some neighborhood of  $x_c$ . (However, the converse is not true; there are degenerate critical points which are isolated).

(a) If all the eigenvalues are positive, we have an isolated minimum at  $x_c$ .

(b) If all the eigenvalues are negative, we have an isolated maximum at  $x_c$ .

(c) If some eigenvalues are positive and some are negative, we have an isolated saddle at  $x_c$ .

(2) One or more of the eigenvalues of  $Hf|_{x_c}$  vanish [i.e.,  $\det(Hf|_{x_c}) = 0, r < n, m > 0$ ]. In this case we have a degenerate critical point. The corank  $m$  is equal to the number of independent "directions" in which the critical point is degenerate.

A degenerate critical point is *structurally unstable* which means that by adding a small perturbation to our function  $f$  we may change the behavior at  $x_c$  drastically. For example  $f = x^4$  has an isolated but degenerate minimum at  $x = 0$ , while  $f = x^4 - \epsilon x^2, \epsilon > 0$  has a (nondegenerate) maximum there. Physically this means, for example, that by taking into account attenuation, or the size of the object more realistically (which amounts to the introduction of new parameters in our potential  $\tilde{U}$ ), we may modify the nature of the degenerate critical points of  $\tilde{U}$ . By contrast, it can be shown that a nondegenerate critical point is *structurally stable*. That is, a small perturbation will not alter the behavior of  $f$  at  $x_c$ . Except for the case of one variable where the type of critical point is determined by the first nonzero derivative of  $f$  (if it exists), the general theory of degenerate critical points of functions of several variables is rather involved, and we refer the interested reader to established references in this field.<sup>26,27</sup> The best policy in such situations is to investigate the nature of the critical point by computer.

As an illustration of the above ideas, consider the situation for the rectangular geometry discussed in Sec. II, Eqs. (16)–(18). The off-diagonal elements of  $H\tilde{U}|_{\bar{x}_c}$  with  $\bar{x}_c$  given by Eq. (18), vanish. Thus the diagonal elements  $\partial^2 \tilde{U} / \partial \bar{x}_i^2$ ,

$\partial^2 \tilde{U} / \partial \bar{y}^2, \partial^2 \tilde{U} / \partial \bar{z}^2$ , evaluated at  $\bar{x}_c$ , are the eigenvalues of  $H\tilde{U}|_{\bar{x}_c}$ . We have

$$\frac{\partial^2 \tilde{U}}{\partial \bar{x}_i^2} \Big|_{\bar{x}_c} = (-1)^{m_x+1} \left( \frac{k_x}{k} \right)^2 g(m_y, m_z). \quad (\text{A5})$$

To obtain  $\partial^2 \tilde{U} / \partial \bar{y}^2$  and  $\partial^2 \tilde{U} / \partial \bar{z}^2$ , simply interchange  $x \leftrightarrow y$  and  $x \leftrightarrow z$ , respectively, in Eq. (A5). The function  $g$  has the following properties:

$$\begin{aligned} g(m_y, m_z) &= 0, & \text{for } m_y, m_z \text{ both odd,} \\ g(m_y, m_z) &= - \left( \frac{f_2}{k^2} \right) \begin{Bmatrix} k_y^2 \\ k_z^2 \end{Bmatrix}, & \text{for } m_y \text{ odd, } m_z \text{ even,} \\ & & \text{for } m_z \text{ odd, } m_y \text{ even,} \\ g(m_y, m_z) &= \frac{2f_1}{3} + \left( \frac{k_x}{k} \right)^2 f_2, & \text{for } m_y, m_z \text{ both even.} \end{aligned} \quad (\text{A6})$$

Let us assume, for example, that  $n_x, n_y, n_z \neq 0$ , and  $f_1, f_2 > 0$ . We then have the following cases:

(1) At least two of the  $m_i$  values are even. Then all three eigenvalues are nonvanishing and we have a nondegenerate critical point.

(a) If all three  $m_i$  values are even, then all three eigenvalues are negative and we have a maximum.

(b) If only two of the  $m_i$  values are even, then all three eigenvalues are positive and we have a minimum.

(2) At least two of the  $m_i$  values are odd. Then at least one eigenvalue vanishes and we have a degenerate critical point.

(a) If all three  $m_i$  values are odd, then all three eigenvalues vanish. In the (111) and (222) rectangular modes, which were investigated by computer for the above choice of  $f_1$  and  $f_2$ , this type of critical point turned out to be a maximum.

(b) If only two of the  $m_i$  values are odd, then one eigenvalue vanishes, and the other two are negative. Here again a computer analysis would provide the simplest means of deciding whether the critical point is a maximum or a "saddle."

Now suppose that  $n_y = 0$ . Then  $\partial \tilde{U} / \partial \bar{y} = \partial^2 \tilde{U} / \partial \bar{y}^2 = 0$  for all  $\bar{y}$ , and consequently we have *nonisolated* critical points. Consider, for example, the (102) rectangular mode and choose  $m_x = 1$  and  $m_z = 2$  ( $m_y$  has to be equal to zero). Then, for  $f_1, f_2 > 0$ ,  $\partial^2 \tilde{U} / \partial \bar{x}^2 > 0$ , and  $\partial^2 \tilde{U} / \partial \bar{z}^2 > 0$ , and we have a *line of minima* in the  $y$  direction at  $x/l_x = z/l_z = 0.5$  (see Fig. 3). Tables V and VIII list the various types of surfaces of nonisolated critical points obtained in the cylindrical and spherical geometries, respectively.

Since we only need to know the *sign* of the eigenvalues of  $Hf|_{x_c}$  and not their actual values, sometimes we are able to deduce the type of critical point by looking at  $\text{tr}(Hf|_{x_c})$  and  $\det(Hf|_{x_c})$ . For example, if  $\text{tr}(Hf|_{x_c}) < 0$ , the critical point cannot be a minimum. If  $\text{tr}(Hf|_{x_c}) < 0$  while  $\det(Hf|_{x_c}) < 0$ , we must have a (nondegenerate) saddle. Now suppose  $\text{tr}(Hf|_{x_c}) < 0$ , but  $\det(Hf|_{x_c}) > 0$ , and the number of variables involved is odd (i.e.,  $n$  is odd); again the critical point at  $x_c$  has to be a (nondegenerate) saddle. On the other hand, if  $n$  is even, the critical point may be a saddle or a maximum.

The *index*  $I$  of  $f$  or  $Hf|_{x_c}$  at a nondegenerate critical point  $x_c$  is equal to the number of *negative* eigenvalues of  $Hf|_{x_c}$ . The index characterizes the type of critical point. For

example, for a  $n \times n$  (nondegenerate) Hessian,  $I = 0$  means a minimum,  $I = n$  means a maximum, and  $0 < I < n$  means a saddle. Both the index  $I$  and the corank  $m$  are invariant numbers under differentiable invertible coordinate changes (diffeomorphisms).<sup>26</sup> Therefore, if  $f$  has, for example, a nondegenerate minimum at  $x_c$  and we perform a diffeomorphism  $\bar{x} = \bar{x}(x)$ , the transformed  $f$  will have a nondegenerate minimum at the corresponding position  $\bar{x}_c = \bar{x}(x_c)$ . However, one has to be careful, as the following simple example illustrates. Consider the elliptic paraboloid given by  $f(x,y) = x^2 + t^2 y^2$ .  $f$  has a nondegenerate minimum at  $x = y = 0$  for  $t \neq 0$ , since

$$Hf|_{x=0, y=0} = \begin{pmatrix} 2 & 0 \\ 0 & 2t^2 \end{pmatrix}. \quad (\text{A7})$$

If we change to polar coordinates, we have  $f = F(r, \phi) = r^2(\cos^2 \phi + t^2 \sin^2 \phi)$ . Now  $\partial F / \partial r = \partial F / \partial \phi = 0$  for  $r = 0$  and any  $\phi$ , and

$$Hf|_{r=0} = \begin{pmatrix} 2 \cos^2 \phi + 2t^2 \sin^2 \phi & 0 \\ 0 & 0 \end{pmatrix}, \quad (\text{A8})$$

which seems to imply that now we have a degenerate critical point at  $r = 0$ . The paradox is resolved when we realize that the Jacobian determinant of the transformation from Cartesian to polar coordinates is equal to  $r$  and hence the transformation is *not invertible* at  $r = 0$ . In our investigation of the spherical geometry (Sec. IV),

$$\frac{\partial \tilde{U}}{\partial \xi} = \frac{\partial \tilde{U}}{\partial \theta} = \frac{\partial \tilde{U}}{\partial \phi} = 0 \quad (\text{A9})$$

at  $\xi = 0$  for all  $l$  and  $m$ , where  $\xi = k_l r$ . So  $\xi = 0$  is always a critical point of  $\tilde{U}(\xi, \theta, \phi)$ . If we let  $(lm) \rightarrow (1n0)$ , the  $\phi$  dependence drops out and  $\tilde{U} = \tilde{U}(\xi, \theta)$ . Now

$$\frac{\partial^2 \tilde{U}}{\partial \xi \partial \theta} = \frac{\partial^2 \tilde{U}}{\partial \theta^2} = 0, \quad \frac{\partial^2 \tilde{U}}{\partial \xi^2} = A(k, \theta) > 0 \quad (\text{A10})$$

at  $\xi = 0$ , for all  $k$  and  $\theta$  ( $f_1, f_2 > 0$ ). This is a nondegenerate minimum as in the previous example, and it is better to think of  $\theta$  here as a "parameter" rather than an independent variable so that the relevant  $H\tilde{U}$  consists of  $\partial^2 \tilde{U} / \partial \xi^2$  only.

## APPENDIX B: EFFECTIVE RESTORING FORCE CONSTANTS

In Appendix B we restrict ourselves to the case of three independent variables, although the results generalize readily to the case of  $n$  variables. In order to make comparisons between the various minima of the potential  $\tilde{U}$  for different modes of the same geometry, or even for different geometries, we introduce the concept of an *effective restoring force constant*  $\bar{\kappa}_i$ . This concept only has meaning for the case of *nondegenerate* minima of the potential. It can be shown that in the neighborhood of a nondegenerate minimum the potential  $\tilde{U}$  may be written, with a proper choice of coordinates  $x_i$ , as the quadratic form

$$\tilde{U} = \frac{1}{2} \sum_{i=1}^3 \bar{\kappa}_i \bar{x}_i^2 + \text{const.}, \quad (\text{B1})$$

where the dimensionless parameters  $\bar{\kappa}_i = \kappa_i / \pi R^3 \rho v_0^2 k^2$  and  $\bar{x}_i = kx_i$ .

This result is a special case of the so-called *Morse lemma*.<sup>27</sup> We give a brief outline of the proof: (a) Translate the coordinate origin to the position of the minimum. (b) Expand  $\tilde{U}$  in a Taylor series about the origin (the minimum). (c) Retain only the first nonvanishing terms; these are the terms involving the second derivatives (since the first derivatives vanish at the minimum). (d) Finally, rotate the coordinate system so as to eliminate cross terms. We now have (B1) which is, of course, identical to the potential energy of a three-dimensional anisotropic harmonic oscillator. The effective restoring force constants  $\bar{\kappa}_i$  are the eigenvalues of the Hessian matrix of  $\tilde{U}$  evaluated at the minimum under consideration (see Appendix A).

The fact that minima of interest are nondegenerate guarantees the existence of the  $\bar{\kappa}_i$  and the convexity of  $\tilde{U}$  near the minimum. Thus by defining the  $\bar{\kappa}_i$  as above, we insure that the smallest  $\bar{\kappa}_i$  is in the direction of the minimum restoring force, the largest in the direction of the maximum restoring force, and so on. If the critical point is not a nondegenerate minimum, some of the  $\bar{\kappa}_i$  may be zero or negative and thus lose their meaning as "restoring force" constants. However, we may still define restoring force constants for certain directions. To see this, we give below a somewhat simplified version of the so-called *splitting lemma*<sup>27</sup> as it applies to our cases. Suppose that  $\tilde{U}$  has a critical point and the Hessian of  $\tilde{U}$  evaluated at this critical point has rank  $r$  (and corank  $3 - r$ ). Then in a neighborhood around this critical point,  $\tilde{U}$  is equivalent to a function of the form

$$\tilde{U} = \left(\frac{1}{2}\right) \sum_{i=1}^r \bar{\kappa}_i \bar{x}_i^2 + \tilde{U}_d(\bar{x}_{r+1}, \bar{x}_3) + \text{const.}, \quad (\text{B2})$$

i.e.,  $\tilde{U}$  may be put in this form by a proper choice of coordinates. If the critical point under consideration is nonisolated, then we assume that Eq. (B2) is evaluated at *one* of the critical points of this nonisolated set. More generally, of course, the  $\bar{\kappa}_i$ 's could be considered as depending on the variable(s) along the direction(s) in which the critical point is nonisolated. We note that the splitting lemma is a generalization of the Morse lemma, and it enables us to deal with degenerate points by "splitting" the function into a Morse (nondegenerate) piece on one set of variables and a degenerate piece on a different set of variables, whose number is equal to the corank. For example, consider again the (102) rectangular mode discussed in Appendix A. We found that under certain conditions  $\tilde{U}$  has a line of minima in the  $y$  direction at  $x/l_x = z/l_z = 0.5$ .  $H\tilde{U}$  evaluated on this set of nonisolated critical points has rank  $r = 2$  and corank  $m = 1$ . Therefore, in the neighborhood of this set of minima, we may write

$$\tilde{U} = \frac{1}{2} \bar{\kappa}_x \bar{x}^2 + \frac{1}{2} \bar{\kappa}_z \bar{z}^2 + \tilde{U}_d(\bar{y}) + \text{const.} \quad (\text{B3})$$

In this example it turns out that  $\tilde{U}_d(\bar{y}) = 0$  since the  $y$  dependence drops out of  $\tilde{U}$  with the choice  $n_y = 0$ . From Eqs. (A5), (A6), etc. we readily find that

$$\bar{\kappa}_x = \left(\frac{k_x}{k}\right)^2 \left[\frac{2f_1}{3} + \left(\frac{k_x}{k}\right)^2\right] f_2, \quad \bar{\kappa}_z = \left(\frac{k_z k_x}{k^2}\right)^2 f_2. \quad (\text{B4})$$

The unimportant constant in (B3) is, of course,  $\tilde{U}(x = 0.5l_x, z = 0.5l_z)$ .



It is rather interesting that the  $\bar{\kappa}_i$ s as defined above are a special case of what are known as the *principal curvatures* of a hypersurface in differential geometry.<sup>28</sup> In our case, they are the principal curvatures at a minimum of the hypersurface defined by  $\bar{U}$ . The sum and product of the  $\bar{\kappa}_i$ s are also useful quantities and, as can be seen from Eqs. (A3) and (A4), they are, respectively, the  $\text{tr}(H\bar{U}|_{\bar{x}_c})$  and  $\text{det}(H\bar{U}|_{\bar{x}_c})$ .

## APPENDIX C: FORCE COMPONENT EXPRESSIONS FOR CYLINDRICAL AND SPHERICAL GEOMETRY

As an aid to computer calculations, we present below the force component expressions for cylindrical and spherical geometry. The force components for rectangular geometry are given by Eq. (16).

In cylindrical geometry, the evaluation of Eqs. (27)–(29) for the  $\bar{F}_r, \bar{F}_\phi,$  and  $\bar{F}_z$  force components yields

$$\begin{aligned} \bar{F}_r = -\frac{\bar{U}}{\partial r} = & -\frac{k_r}{k} \left( 2J_m(\chi) \left[ \left( \frac{m}{\chi} \right) J_m(\chi) - J_{m+1}(\chi) \right] \left[ \left( \frac{f_1}{3} \right) \cos^2 m\phi - \left( \frac{f_2}{2} \right) \left( \frac{mk_r}{k\chi} \right)^2 \right] \cos^2 k_z z \right. \\ & \left. - \left( \frac{f_2}{2} \right) \left( \frac{k_z}{k} \right)^2 \cos^2 m\phi \sin^2 k_z z \right) + \left( \frac{f_2}{\chi} \right) \left( \frac{mk_r}{k\chi} \right)^2 J_m^2(\chi) \cos^2 k_z z + \left( \frac{f_2}{2} \right) \left( \frac{mk_r^2}{k^2 \chi} \right) J_m(\chi) [J_m(\chi) - J_{m+2}(\chi)] \\ & \times \cos^2 m\phi \cos^2 k_z z + \left( \frac{f_2}{2} \right) \left( \frac{k_r}{k} \right)^2 J_{m+1}(\chi) \left[ \left( \frac{2m(m-1)}{\chi^2} - 1 \right) J_m(\chi) \right. \\ & \left. - \left( \frac{2m}{\chi} \right) J_{m+1}(\chi) + J_{m+2}(\chi) \right] \cos^2 m\phi \cos^2 k_z z. \end{aligned} \quad (C1)$$

$$\begin{aligned} \bar{F}_\phi = & \left( \frac{mk_r}{k\chi} \right) \sin 2m\phi \left\{ J_m^2(\chi) \left[ \left( \frac{f_1}{3} \right) \cos^2 k_z z - \left( \frac{f_2}{2} \right) \left( \frac{k_z}{k} \right)^2 \sin^2 k_z z \right] \right. \\ & \left. + \left( \frac{f_2}{2} \right) \left( \frac{k_r}{k} \right)^2 J_{m+1}(\chi) \left[ \left( \frac{2m}{\chi} \right) J_m(\chi) - J_{m+1}(\chi) \right] \cos^2 k_z z \right\}. \end{aligned} \quad (C2)$$

$$\begin{aligned} \bar{F}_z = & \left( \frac{k_z}{k} \right) \sin 2k_z z \left\{ J_m^2(\chi) \left[ \left( \frac{f_1}{3} \right) + \left( \frac{f_2}{2} \right) \left( \frac{k_z}{k} \right)^2 \right] \cos^2 m\phi - \left( \frac{f_2}{2} \right) \left( \frac{mk_r}{k\chi} \right)^2 \right\} \\ & + \left( \frac{f_2}{2} \right) \left( \frac{k_r}{k} \right)^2 J_{m+1}(\chi) \left[ \left( \frac{2m}{\chi} \right) J_m(\chi) - J_{m+1}(\chi) \right] \cos^2 m\phi. \end{aligned} \quad (C3)$$

In spherical geometry, the evaluation of Eqs. (43)–(45) for the  $\bar{F}_r, \bar{F}_\theta,$  and  $\bar{F}_\phi$  force components yields

$$\begin{aligned} \bar{F}_r = & -(2f_1/3\xi) j_l(\xi) [j_l(\xi) - \xi j_{l+1}(\xi)] [P_l^m(\mu)]^2 \cos^2 m\phi - (f_2/\xi^3) A + (f_2/\xi^3) \{ [j_l(\xi) - \xi j_{l+1}(\xi)] \\ & \times [l^2 j_l(\xi) - 2(l+1)\xi j_{l+1}(\xi) + \xi^2 j_{l+2}(\xi)] [P_l^m(\mu)]^2 \cos^2 m\phi + j_l(\xi) [j_l(\xi) - \xi j_{l+1}(\xi)] B / (1-\mu^2) \}. \end{aligned} \quad (C4)$$

$$\begin{aligned} \bar{F}_\theta = & [2/\xi (1-\mu^2)^{1/2}] \{ (f_1/3) j_l^2(\xi) P_l^m(\mu) [(l+1)\mu P_l^m(\mu) - (l-m+1)P_{l+1}^m(\mu)] \cos^2 m\phi \\ & - (f_2/2\xi^2) \{ [j_l(\xi) - \xi j_{l+1}(\xi)]^2 P_l^m(\mu) [(l+1)\mu P_l^m(\mu) - (l-m+1)P_{l+1}^m(\mu)] \cos^2 m\phi \\ & + j_l^2(\xi) \mu B / (1-\mu^2) + j_l^2(\xi) / (1-\mu^2) \{ [(l+1)\mu P_l^m(\mu) - (l-m+1)P_{l+1}^m(\mu)] [(l+1)(1+\mu^2) \\ & - (l+m+1)(l-m+1)] P_l^m(\mu) \cos^2 m\phi + m^2 P_l^m(\mu) [(l+1)\mu P_l^m(\mu) - (l-m+1)P_{l+1}^m(\mu)] \sin^2 m\phi \} \}. \end{aligned} \quad (C5)$$

$$\begin{aligned} \bar{F}_\phi = & [m \sin 2m\phi / \xi (1-\mu^2)^{1/2}] \{ (f_1/3) j_l^2(\xi) [P_l^m(\mu)]^2 - (f_2/2\xi^2) \{ [j_l(\xi) - \xi j_{l+1}(\xi)]^2 [P_l^m(\mu)]^2 \\ & + [j_l^2(\xi) / (1-\mu^2)] \{ [(l+1)\mu P_l^m(\mu) - (l-m+1)P_{l+1}^m(\mu)]^2 - [m P_l^m(\mu)]^2 \} \}, \end{aligned} \quad (C6)$$

where

$$B = [(l+1)\mu P_l^m(\mu) - (l-m+1)P_{l+1}^m(\mu)]^2 \cos^2 m\phi + [m P_l^m(\mu)]^2 \sin^2 m\phi \quad (C7)$$

and

$$A = [j_l(\xi) - \xi j_{l+1}(\xi)]^2 [P_l^m(\mu)]^2 \cos^2 m\phi + [j_l^2(\xi) / (1-\mu^2)] B. \quad (C8)$$

## APPENDIX D: THE SPACE-TIME-AVERAGED ENERGY DENSITY

In comparing the positioning characteristics of various modes, it is appropriate to assume that each mode has the same space-time-averaged energy density given by<sup>29</sup>

$$\langle \bar{\epsilon} \rangle = \frac{1}{V} \int \left( \frac{\bar{p}_{\text{in}}^2}{2\rho c^2} + \frac{\rho \bar{v}_{\text{in}}^2}{2} \right) dV, \quad (D1)$$

where the overbars denote time averages, and  $V$  is the volume of the chamber. This expression can be simplified to give

$$\langle \bar{\epsilon} \rangle = (\rho v_0^2) N, \quad (D2)$$

where  $N$  is a dimensionless constant,

$$N = \frac{1}{2V} \int (\bar{p}^2 + \bar{v}^2) dV. \quad (D3)$$

The magnitude of  $N$  depends on the geometry and mode.

For rectangular geometries, we can easily integrate Eq. (D3) to obtain

$$N = 2^{-(s+1)}, \quad (D4)$$

where  $s$  is equal to the number of nonzero quantum numbers.

For cylindrical geometries, (D3) gives us

$$\begin{aligned} N = & \{ 2^{-(s+2)} / \pi^2 [\alpha_{mn}^2 + (a/l_z)^2 n_z^2] \} \\ & \times \{ (2m + \pi^2 [\alpha_{mn}^2 + 2(a/l_z)^2 n_z^2] \\ & \times (1 - m^2 / \pi^2 \alpha_{mn}^2)) J_m^2(\pi \alpha_{mn}) \\ & + [\pi^2 \alpha_{mn}^2 - (m+1)^2] J_{m+1}^2(\pi \alpha_{mn}) \}, \end{aligned} \quad (D5)$$

where

$$s' = 2 \text{ if } m \neq 0, \quad n_z \neq 0,$$

$$s' = 1 \text{ if } m = 0 \text{ and } n_z \neq 0, \text{ or } m \neq 0 \text{ and } n_z = 0,$$

$$s' = 0 \text{ if } m = n_z = 0.$$

Finally, for *spherical geometries*, we find

$$N = \left( \frac{3(2^{-(s'+2)})(l+m)!}{(2l+1)(l-m)!} \right) \left[ \left( 1 + \frac{l}{\pi^2 \gamma_{ln}^2} \right) j_l^2(\pi \gamma_{ln}) + \left[ j_{l+1}(\pi \gamma_{ln}) - \left( \frac{2(l+1)}{\pi \gamma_{ln}} \right) j_l(\pi \gamma_{ln}) \right] j_{l+1}(\pi \gamma_{ln}) \right], \quad (D6)$$

where  $s'' = 1$  if  $m \neq 0$  and  $s'' = 0$  if  $m = 0$ .

<sup>1</sup>A. Kundt, "Ueber eine neue Art akustischer Staubfiguren und über die Anwendung derselben zur Bestimmung der Schallgeschwindigkeit in festen Körpern und Gasen," *Annal. Phys.* **127**, 497 (1866).

<sup>2</sup>L. V. King, "On the Acoustic Radiation Pressure on Spheres," *Proc. R. Soc. London Ser. A* **147**, 212 (1934).

<sup>3</sup>K. Yosioka and Y. Kawasima, "Acoustic Radiation Pressure on a Compressible Sphere," *Acustica* **5**, 167 (1955).

<sup>4</sup>E. Klein, "Absolute Sound Intensity in Liquids by Spherical Torsion Pendula," *J. Acoust. Soc. Am.* **9**, 312-320 (1938).

<sup>5</sup>I. Rudnick, "Measurements of the Acoustic Radiation Pressure on a Sphere in a Standing Wave Field," *J. Acoust. Soc. Am.* **62**, 20-22 (1977).

<sup>6</sup>E. Leung, N. Jacobi, and T. Wang, "Acoustic Radiation Force on a Rigid Sphere in a Resonance Chamber," *J. Acoust. Soc. Am.* **70**, 1762-1767 (1981).

<sup>7</sup>T. F. W. Embleton, "Mean Force on a Sphere in a Spherical Sound Field. I (Theoretical)," *J. Acoust. Soc. Am.* **26**, 40-45 (1954).

<sup>8</sup>T. F. W. Embleton, "The Radiation Force on a Spherical Obstacle in a Cylindrical Sound Field," *Can. J. Phys.* **34**, 276 (1956).

<sup>9</sup>L. P. Gor'kov, "On the Forces Acting on a Small Particle in an Acoustic Field in an Ideal Fluid," *Sov. Phys. Dokl.* **6**, 773 (1962); translated from *Dok. Akad. Nauk SSSR* **140**, 88 (1961).

<sup>10</sup>W. L. Nyborg, "Radiation Pressure on a Small Rigid Sphere," *J. Acoust. Soc. Am.* **42**, 947-952 (1967).

<sup>11</sup>*High-Intensity Ultrasonic Fields*, edited by L. D. Rosenberg (Plenum, New York, 1971).

<sup>12</sup>*Physical Principles of Ultrasonic Technology*, edited by L. D. Rosenberg (Plenum, New York, 1973), Vols. 1,2.

<sup>13</sup>M. Barmatz, "Overview of Containerless Processing Technologies," in *Proceedings of the Symposium of Materials Processing in the Reduced Gravity Environment of Space*, Boston, MA, November 1981 (Elsevier, New York, 1982), p. 25.

<sup>14</sup>M. Barmatz and P. Collas, "Acoustic Radiation Force on a Sphere in Plane, Cylindrical and Spherical Standing Wave Fields," in *Proceedings of the 11th International Congress on Acoustics*, Paris, France, 1983, Vol. 1, p. 245.

<sup>15</sup>Two additional conditions are involved:  $R$  must be large in comparison with the displacement amplitude of the fluid particles in the wave, since otherwise the fluid is not generally in potential flow; thus we require  $R \gg v_0/\omega$ . Also,  $R \gg \sqrt{\eta/\omega\rho}$ , where  $\eta$  is the viscosity of the medium.

<sup>16</sup>L. D. Landau and E. M. Lifshitz, *Fluid Mechanics* (Pergamon, New York, 1959); see in particular Secs. 73 and 76.

<sup>17</sup>See Ref. 16, problem 2 of Sec. 76, p. 297.

<sup>18</sup>Gor'kov omits most of the algebra; there are also some misprints, so the reader is advised to compare with the Russian version of Ref. 9.

<sup>19</sup>We found two misprints in Embleton's Eq. (34): The second right-hand side term should be  $0.05556\alpha^6$  (instead of  $0.05445\alpha^6$ ) and the sixth right-hand term should be  $0.6667\alpha^3$  (instead of  $0.6599\alpha^3$ ). Embleton's radiation force  $\bar{P}$  is the negative of our  $F = -\text{grad } U$ .

<sup>20</sup>P. M. Morse, *Vibration and Sound* (McGraw-Hill, New York, 1948), 2nd ed.

<sup>21</sup>T. G. Wang, M. M. Saffren, and D. D. Elleman, "Acoustic Chamber For Weightless Positioning," AIAA paper #74-155 (1974). This technique was successfully demonstrated on the STS 11 space shuttle flight, February, 1984.

<sup>22</sup>Experimentally, the phase constant  $\phi_0$  is usually specified by the way the resonator is excited into resonance.

<sup>23</sup>The phase constants  $\phi_0$  and  $\theta_0$  have been arbitrarily set to zero.

<sup>24</sup>H. G. Ferris, "The Free Vibrations of a Gas Contained Within a Spherical Vessel," *J. Acoust. Soc. Am.* **24**, 57-61 (1952).

<sup>25</sup>Stable acoustic positioning was experimentally demonstrated by one of us (MB) using a rectangular (221), cylindrical (011) and (102), and a spherical (100) single-mode levitator.

<sup>26</sup>V. I. Arnold, "Critical Points of Smooth Functions and Their Normal Forms," *Russ. Math. Surv.* **30**(5), 1 (1975), translated from *Usp. Mat. Nauk* **30**(5),3 (1975); "Normal Forms of Functions in Neighborhoods of Degenerate Critical Points," *Russ. Math. Surv.* **29**(2),10 (1974), translated from *Usp. Mat. Nauk* **29**(2),11 (1974).

<sup>27</sup>See, for example, T. Poston and I. Stewart, *Catastrophe Theory and Its Applications* (Pitman, San Francisco, 1978), Chap. 4.

<sup>28</sup>The interested reader is referred to *Morse Theory* by J. Milnor, *Annu. Stud.* **51** (Princeton U. P., Princeton, NJ, 1963), p. 34. A pertinent discussion is given also in a clear early paper by E. Kasner, *Am. J. Math.* **43**, 126 (1921); see his Eq. (9) and below.

<sup>29</sup>See, for example, Ref. 16, p. 250.